Orbital pacing of the Early Jurassic carbon cycle, black-shale formation and seabed methane seepage

WEIMU XU[1]*, MICHA RUHL[1], STEPHEN P. HESSELBO[2], JAMES B. RIDING[3] and HUGH C. JENKYNS[1]

[1]*Department of Earth Sciences, University of Oxford, Oxford OX1 3AN, UK (*Correspondence: weimu.xu@earth.ox.ac.uk)*

[2]*Camborne School of Mines, University of Exeter, Penryn TR10 9FE, UK*

[3]*British Geological Survey, Keyworth, Nottingham NG12 5GG, UK*

ABSTRACT

The Early Jurassic (~201–174 Ma) was marked by a series of rapid perturbations in climate, the environment, and global geochemical cycles, which have been linked to volcanic outgassing and the release of biogenic or thermogenic methane into the ocean–atmosphere system. The state of the global carbon cycle and prevailing climatic and environmental conditions that existed at this time are, however, poorly constrained. Here, mudrocks of the Lower Sinemurian *Arietites bucklandi* ammonite Biozone at coastal exposures at Kilve, Somerset, UK have been studied. This succession includes laminated organic-rich black shales, which are present throughout the Bristol Channel Basin, and coincides with a 2–3‰ negative carbon-isotope excursion, distinct changes in inferred land vegetation, and abundant marine prasinophytes (green algae). The event itself does not represent a single perturbation of the regional environment, but follows in a sequence of eccentricity-modulated, precession-paced perturbations that occur throughout the preceding Hettangian stage, with the periodic formation of organic-rich laminated black shales in the Bristol Channel Basin. However, the Early Sinemurian event studied herein is more extreme in nature, with sedimentary total organic carbon (TOC) values of 5–11% persisting over ~2 m, representing ~100 kyr, possibly in phase with short (~100 kyr) and long (~405 kyr) eccentricity forcing. The formation of methane-seep carbonate-cemented mounds took place relatively soon after the deposition of laminated black shales. Biogenic methane probably formed in response to microbial

methanogenesis in the organic-rich black shale, which was subsequently channeled to the sediment-water interface approximately 5 m above the source bed, and ~200 kyr after cessation of formation of the black shale.

Keywords Early Jurassic, Sinemurian, *A. bucklandi* ammonite Biozone, carbon-cycle perturbation, astronomical forcing, methane seepage.

[1] INTRODUCTION

The Early Jurassic (~201–174 Ma) was punctuated by several major and minor fluctuations in climate, palaeoenvironment, and global geochemical cycles (Jenkyns *et al*., 2002; Dera *et al*., 2011; Korte and Hesselbo, 2011; Ullmann *et al*., 2014; Brazier *et al*., 2015). The most significant of these perturbations, the Early Toarcian Oceanic Anoxic Event (T-OAE, at ~183Ma) (Jenkyns, 1985, 1988), was characterized by a globally observed negative carbon-isotope excursion (CIE) of as much as ~7‰ in marine and terrestrial organic matter and a 3–6‰ negative excursion in coeval carbonate and biomarker compounds (Hesselbo *et al*., 2000, 2007; Jenkyns *et al*., 2002; Kemp *et al.*, 2005; Hermoso *et al*., 2009; Schouten *et al*., 2000; French *et al.*, 2014; Suan *et al*., 2015). This negative shift, which is interposed within an overarching positive excursion, likely resulted from input of isotopically light carbon from volcanic outgassing and/or the release of isotopically depleted biogenic or thermogenic methane into the ocean–atmosphere system (Duncan *et al*., 1997; Hesselbo *et al*., 2000; Jenkyns, 2003; Kemp *et al*., 2005; McElwain *et al*., 2005; Svensen *et al.*, 2007). Palaeoclimatic and palaeoenvironmental change at this time led to the widespread development of oceanic anoxia and euxinia via elevated nutrient supply, marine primary productivity and water-column stratification. Enhanced productivity and preservation of sedimentary organic matter led to the increased burial of organic matter in marine and, potentially, lacustrine environment and caused the overarching positive carbon-isotope excursion due to preferential burial of isotopically light carbon (Jenkyns, 2010). The T-OAE has now been extensively studied and has been recognized in both hemispheres (Jenkyns,

1988; Jenkyns *et al*., 2002; Hesselbo et al., 2007; Al-Suwaidi *et al*., 2010, 2016). However, several recent studies have demonstrated that the T-OAE was preceded by smaller magnitude global carbon-cycle changes, during the Early Jurassic, in the Late Sinemurian (*Asteroceras obtusum* to *Oxynoticeras oxynotum* ammonite biozones), and at the Sinemurian–Pliensbachian and the Pliensbachian–Toarcian stage boundaries (Hesselbo *et al*., 2007; Littler *et al.*, 2010; Korte and Hesselbo, 2011; Jenkyns and Weedon, 2013; Riding *et al*., 2013; Duarte *et al.*, 2014; Porter *et al.*, 2014).

A 2–3‰ negative CIE in bulk organic matter was previously observed for the Early Sinemurian *A. bucklandi* ammonite Biozone (*Coroniceras rotiforme* ammonite Subbiozone) at East Quantoxhead (Somerset, UK) (Ruhl *et al*., 2010; Hüsing *et al*., 2014). This negative excursion in $\delta^{13}C_{TOC}$ is associated with an interval of laminated black shale, with elevated total organic carbon (TOC) values of up to ~8%, suggesting at least local/basinal changes in the depositional environment. The nature of this environmental change and its relation to the global carbon cycle have, however, not been investigated previously. Furthermore, the *A. bucklandi* ammonite Zone at Kilve, Somerset, is also marked by methane seepage and the associated formation of large (~1.5 m) conical mounds or mud volcanoes (Cornford, 2003; Allison *et al*., 2008; Price *et al*., 2008). The present contribution addresses (1) a potential Early Sinemurian global carbon-cycle perturbation and palaeoenvironmental change leading to black-shale deposition in the Bristol Channel Basin; (2) its link to the orbital pacing of Early Jurassic climate; and (3) the subsequent genesis of the Early Jurassic seabed methane seepage. We also include new observations on recently reported methane seep carbonates from the Lower Jurassic (Toarcian) of Yorkshire, which serve as a comparative example.

[2] GEOLOGICAL BACKGROUND

[2.1] Origin of sedimentary rhythms and total organic-carbon enrichment in the Blue Lias Formation of Somerset

The Early Jurassic Bristol Channel Basin was part of the Laurasian Seaway, and was marked by a generally progressive marine transgression, including a terrestrial to marine transition,

during the latest Triassic (Fig. 1; Hesselbo, 2008). The Lower Jurassic Blue Lias Formation formed during a phase of rapid flooding, and resulted in the periodic development of organic-rich laminated black shales (Hallam, 1995, 1997; Warrington *et al*., 2008). The relatively deeper marine (shelf) sediments of the Hettangian and Sinemurian Blue Lias Formation overlie the shallow-marine Lilstock Formation which is Rhaetian (latest Triassic) in age (Richardson, 1911; Whittaker and Green, 1983; Cox *et al*., 1999; Warrington *et al.*, 2008). The *A. bucklandi* ammonite Zone may be marked by a relative sea-level fall, reaching a lowstand in the *C. rotiforme* ammonite Subzone (Hesselbo and Jenkyns, 1998; Hesselbo and Coe, 2000; Hesselbo, 2008).

The Blue Lias Formation has been subject to extensive stratigraphical studies (e.g. Hallam, 1964, 1987; Weedon, 1986; Smith, 1989; McRoberts and Newton, 1995; Weedon *et al.*, 1999; Hesselbo *et al.*, 2002; Deconinck *et al.*, 2003; Hounslow *et al.*, 2004; Mander and Twitchett, 2008; Korte *et al.*, 2009; Bonis *et al.*, 2010; Clémence *et al.*, 2010; Ruhl *et al.*, 2010; Bonis and Kürchner, 2012; Hüsing *et al.*, 2014). Locally, at the North Somerset coast, the Blue Lias Formation defined in Cox *et al.* (1999) has been subdivided into Aldergrove Beds, St Audries Shales, Blue Lias, Kilve Shales, Quantocks Beds, Doniford Shales and Helwell Marls (Palmer, 1972). This major lithostratigraphical unit with regional extent comprises alternations of limestone and marl/shale beds on the Somerset coast (Ruhl *et al.*, 2010). Limestone beds (10–20 cm thick, locally up to 50 cm thick) are mostly micritic mudstone to wackestone. The limestone beds are fine-grained, and contain varying proportions of clay minerals and micrite (Paul *et al.*, 2008), which probably settled from suspension (Weedon, 1986). Some limestone beds are also concretionary (Hallam, 1986; Weedon, 1986). The limestone beds of the Blue Lias Formation alternate with beds of grey marl and organic-rich laminated black shale (Hallam, 1964, 1986; Campos and Hallam, 1979; Hallam, 1986; Paul *et al.*, 2008), which variably contain terrigenous clay minerals and marine- and terrestrially-derived organic matter (Weedon 1986; Clémence *et al*., 2010). The sedimentary rhythms in the Blue Lias Formation consist of laminated black shale grading into dark or pale grey marl, commonly with concretionary to tabular micritic limestone, which has

been suggested to be diagenetic in origin (Hallam, 1964; Paul *et al.*, 2008). These sedimentary rhythms are not always complete either because organic-rich shale or marl/limestone beds are not everywhere developed, or because the carbonate-rich sediments were diagenetically altered (Ruhl *et al.*, 2010). The origin of cyclic sedimentation in the Blue Lias Formation has been much discussed in the literature (Hallam, 1964, 1986; Campos and Hallam, 1979; Weedon, 1986; Bottrell and Raiswell, 1989; Smith, 1989; Waterhouse, 1999; Paul *et al.*, 2008).

The geographical extent of the limestone-shale couplets indicates chronostratigraphical significance and hence a stable allogenic forcing mechanism likely to be high-frequency climate control (Weedon, 1986; Smith, 1989). Integrated stratigraphical and palaeomagnetic studies on the Blue Lias Formation of Somerset demonstrate that the sedimentary rhythms, with the periodic formation of laminated organic-rich black shale, directly reflect orbitally controlled changes in the depositional environment at ~20 kyr precession periodicities, modulated by the short and long eccentricity cycles (Bonis *et al.*, 2010; Ruhl *et al.*, 2010; Hüsing *et al.*, 2014). Periodically enhanced TOC values in the Hettangian and the lowermost Sinemurian Blue Lias Formation, with values of up to 10%, are especially high at the base of the *P. planorbis* ammonite Zone, the middle of the *A. liasicus* ammonite Zone and the *S. angulata–A. bucklandi* ammonite zone boundary, probably in response to 405 kyr (and potentially ~2 Myr) modulated, precession-controlled changes in the palaeo-depositional environment (Ruhl *et al.*, 2010; Hüsing *et al.*, 2014; Sha *et al.*, 2015).

Black shales from the *A. bucklandi* ammonite Zone at Kilve have previously been categorized as oil shale, albeit of rather low quality (Gallois, 1979). A 2-m-thick black-shale interval, with TOC >10%, in the *A. bucklandi* ammonite Zone in East Quantoxhead is marked by a ~2.5‰ negative excursion in $\delta^{13}C_{TOC}$ (Ruhl *et al*., 2010). Lower in the stratigraphy, 1–2‰ fluctuations in $\delta^{13}C_{TOC}$ in the Hettangian and the Sinemurian succession of St Audries Bay and East Quantoxhead in Somerset potentially reflect changes in the global exogenic carbon cycle, on Milankovitch periodicities (Clémence *et al.*, 2010; Ruhl *et al.*, 2010; Hüsing *et al.*, 2014). Alternatively, these periodic alternations in $\delta^{13}C$ may express changes in

143 sedimentary organic-matter source, changes in the magnitude of marine and/or terrestrial
144 fractionation for ^{12}C, and/or changes in the basinal isotopic composition of the dissolved
145 inorganic carbon (DIC) pool in response to changes in basin hydrography. The orbitally paced
146 deposition of laminated black shale at this time was probably in response to changes in both
147 productivity and preservation, likely due to enhanced nutrient (and terrestrial organic-matter)
148 supply and water-column stratification resulting from precession-controlled changes in the
149 hydrological cycle modulated by eccentricity (Bonis *et al.*, 2010; Clémence *et al.*, 2010; Ruhl
150 *et al.*, 2010).

151 The Kilve coastal cliff section studied here is located west of Bridgwater and the River
152 Parrett on the Somerset coast, UK, ~500 m east of Kilve Beach and ~1 km north of Kilve
153 village (Fig. 1). The exposure at Kilve covers the stratigraphical interval of the *A. bucklandi*
154 ammonite Zone with laminated black shale (with TOC up to ~10%), similar to as previously
155 observed at East Quantoxhead (Fig. 2). The foreshore outcrop is also marked by conical seep
156 mounds (mud volcanoes) occurring at a single stratigraphical level that overlies this high-
157 TOC black-shale interval by ~5 m (Figs 2, 3 and 4) (Whittaker and Green, 1983; Cornford,
158 2003; Allison *et al*., 2008; Price *et al*., 2008). The cliff section sampled herein is ~50 m west
159 of the nearest visible seep mound on the foreshore.

160

161 [2.2] **Early Jurassic chronostratigraphy**

162 The age of the Triassic–Jurassic boundary is radiometrically constrained at 201.36 ± 0.17 Ma
163 in the Pucara Basin, Peru (Schaltegger *et al.*, 2008; Schoene *et al.*, 2010; Wotzlaw *et al.*,
164 2014), and astrochronologically constrained at 201.42 ± 0.022 Ma in the Newark/Hartford
165 Basins, USA (Blackburn *et al.*, 2013). The duration of the Hettangian Stage has previously
166 been estimated using cyclostratigraphy at > ~1.29 Myr, from the relatively incomplete marine
167 Blue Lias Formation succession in Dorset and Devon, Southwest England, or at ~2.86 Myr
168 based on an assumed constant linear Early Jurassic decrease in seawater $^{87}Sr/^{86}Sr$ ratios
169 (Weedon *et al.*, 1999). More recent estimates suggest a duration of ~1.7−1.9 Myr, based on
170 the astronomical interpretation of periodically occurring laminated black shales and

systematic fluctuations in organic and inorganic geochemical proxy records in the relatively expanded Blue Lias Formation in Somerset (Ruhl *et al.*, 2010; Hüsing *et al.*, 2014). This duration is further supported by palaeomagnetic correlation to the Geomagnetic Polarity Time Scale (GPTS) of the Newark Basin, USA (Hüsing *et al.*, 2014), and a 199.43 (±0.10) Ma $^{238}U/^{206}Pb$ age for the base Sinemurian in the Pucara Basin of Peru (Schaltegger *et al.*, 2008; Guex *et al.*, 2012). The integrated bio-, cyclo- and magnetostratigraphic framework for the Blue Lias Formation, combined with radiometric dating, directly constrains the age and duration of changes in the depositional environment in the Early Jurassic Bristol Channel Basin.

[2.3] **Early Sinemurian methane seeps**

Several large, conical mounds, interpreted as mud volcanoes, have been observed in a foreshore outcrop east of Kilve Beach in western Somerset, occurring at a discrete level within the Kilve Shales (division of Palmer, 1972) in the *C. rotiforme* ammonite Subzone of the *A. bucklandi* ammonite Zone (Whittaker and Green, 1983; Cornford, 2003; Allison *et al.*, 2008; Price *et al.*, 2008). These mounds are up to 1 m high and up to 3 m in diameter, and their flanks are formed by a limestone shell, which is composed of micritic carbonate and includes pods and sheets of bioclasts and intraclasts (Allison *et al.*, 2008). The shape of ammonites and intraclasts on the flanks of the mounds suggests cementation close to the sediment–water interface, prior to compaction (Allison *et al.*, 2008). This mound-forming level is interpreted as being largely oxygen-deficient because of the scarcity of benthic biota, except for one of the mounds, where benthic foraminifera (*Involutina liassica)*, bivalves, crinoidal fragments and gastropods, are present (Allison *et al.*, 2008; Price *et al.*, 2008). The abundance of the benthic foraminifer *Involutina liassica* in one mound indicates at least brief episodes of oxygenation (Allison *et al.*, 2008; Price *et al.*, 2008). The mound-forming authigenic carbonate (cf. Liang *et al.*, 2016) has depleted carbon-isotope signatures of –11.5‰ to –32.3‰ and such ^{12}C-enriched signatures have been interpreted to originate from anaerobic

methane oxidation, and mixing of the liberated carbon with seawater DIC (Allison *et al*., 2008; Price *et al*., 2008).

Early Jurassic seep mounds have previously been observed in several localities in Europe, including an Upper Pliensbachian outcrop in southern France (van de Schootbrugge *et al.*, 2010), and a Lower Toarcian coastal Jet Rock outcrop at Ravenscar, Yorkshire, UK (Fig. 4; Hesselbo *et al*., 2013). The shape and lithological composition of the conical mounds at Ravenscar are similar to the ones on the foreshore of the Kilve coast.

[3] MATERIALS AND METHODS

[3.1] Materials

[3.1.1] The Early Sinemurian *A. bucklandi* ammonite Zone at Kilve

In this study, 15.6 m of mudstone and laminated black shale of the Early Sinemurian *A. bucklandi* ammonite Zone (*C. rotiforme* ammonite Subzone) was sampled at 10- to 11-cm resolution at the coastal cliff outcrop east of Kilve Beach (Figs 3 and 4; 51°11'39.4"N, 3°13'00.8"W). The logged and sampled interval covers the sedimentary sequence between and including beds C121 and E1 (division of Palmer, 1972), in the Blue Lias Formation (Cox *et al.*, 1999). The interval sampled is stratigraphically coeval with the 2–3‰ negative CIE as observed in the middle of the *A. bucklandi* ammonite Zone at East Quantoxhead and it also spans the stratigraphic horizon with methane seep occurrence, ~5 m above the top of the laminated black shale (Fig. 2; Ruhl *et al.*, 2010). In the cliff section, samples were only collected from the grey mudstones and the laminated black shales but not from the locally developed concretionary limestone beds.

The base of the sampled outcrop is marked by alternations of limestones and marly mudstones containing complete and fragmentary macrofossils, including ammonites, bivalves and crinoids (Figs 3 and 4). There is a ~2 m thick (Figs 3 and 4), laminated black shale with little bioturbation and sparse ammonite fossils at a stratigraphical height of 3.7–5.5 m. The trace fossil *Diplocraterion* appears close to the top of the black-shale interval (Figs 3 and 4). Strata overlying the laminated black-shale interval consist of alternating marl and shale beds,

with a few discrete nodular limestone beds. This interval has yielded ammonites, bivalves and crinoids. Coalified wood fragments of up to 10 cm in length occur throughout, especially in the black shale beds (Figs 3 and 4).

[3.1.2] **Lower Toarcian conical seep mounds at Ravenscar**

Conical seep mounds in the Lower Toarcian Upper Jet Rock at Ravenscar (Yorkshire; 54°24'29.3''N, 0°29'32.7''W) occur stratigraphically above the high TOC (~15%) Lower Jet Rock in the *H. exaratum* ammonite Subzone by ~3 m (Hesselbo *et al.*, 2013). 14 Samples were collected from several carbonate mounds on the foreshore for carbon- and oxygen-isotope analysis in order to test the origin of the seep formation during sub-seafloor gas venting (Fig. 4).

[3.2] **Methods**

Total Carbon (TC) and Total Inorganic Carbon (TIC) were determined for all the studied samples using a Strohlein Coulomat 702 Analyser (Firma Ströhlein Gmbh, Kaarst, Germany) at the Department of Earth Sciences, University of Oxford. For TIC analyses, ~120 mg of powdered sample was roasted overnight at 420 °C to remove the organic matter. Total carbon (~80 mg of powdered sample) and TIC were measured, respectively, on the unroasted and roasted samples, and TOC was the difference between the two. Reproducibility of sample analyses with this method is generally better than 0.1% (Jenkyns 1988). The in-house standard (SAB134; Blue Lias organic-rich marl) was regularly measured. The long-term average value and standard deviation of TOC measurements on the in-house SAB134 standard is 2.95% and 0.069%, respectively.

Organic matter was further characterized by Rock-Eval pyrolysis on a Rock-Eval VI standard instrument (Vinci Technologies, Nanterre, France) with pyrolysis and oxidation ovens, providing Hydrogen Index, Mineral Carbon, Oxygen Index, Residual Organic Carbon, Tmax and TOC. Laboratory procedures as described in Behar *et al.* (2001) were used, and the measurements were all performed at the Department of Earth Sciences, University of Oxford.

Quality control was provided by the in-house SAB134 standard and the certified IFP160000 standard, which were regularly run between samples. The standard deviations on TOC and HI analyses of the in-house SAB134 and the reference IFP160000 standards are, respectively, 0.07% and 0.07% (TOC) and 22.7 mg HC/g TOC and 10.6 mg HC/g TOC (HI).

Analyses of $\delta^{13}C_{TOC}$ were performed on one gram of homogenized sample that was treated with 40 mL cold HCl (3 molar) to dissolve the carbonate. Samples (dissolved in 3 molar HCl) were then put on a hot plate for 2 hours at 60°C. They were subsequently rinsed 4 times with distilled water to reach neutral pH. About 1–15 mg, depending on TOC concentration, of oven-dried and powdered decarbonated sample residue was weighed into 8×5 mm tin capsules for $\delta^{13}C_{TOC}$ analyses. These analyses were performed on a Sercon Europa EA-GSL sample converter connected to a Sercon 20-22 stable-isotope-ratio mass spectrometer (Sercon Limited, Crewe, UK) running in continuous flow mode with a helium carrier gas with a flow rate of 70 ml/min. Carbon-isotope ratios were measured against an internal alanine standard ($\delta^{13}C_{alanine}$ = –26.9‰ ± 0.2‰ V-PDB [Vienna Peedee belemnite]) using a single-point calibration, at the Research Laboratory for Archaeology and History of Art (RLAHA), University of Oxford, UK. The in-house (RLAHA) alanine standard is checked weekly against the certified USGS40, USGS41, and IAEA-CH-6 international reference standards, with a long-term average alanine $\delta^{13}C$ value of -26.92‰ and a standard deviation of 0.15‰.

Analyses of carbonate $\delta^{13}C$ were performed at the Stable Isotope Laboratory at the Open University, Milton Keynes, UK. Bulk samples were dissolved in phosphoric acid on a Thermo Gas Bench II, and C and O isotope analysis was performed on a Thermo Finnegan Delta+ Advantage mass spectrometer (Thermo Fisher Scientific, Waltham, MA, USA). Carbon- and oxygen-isotope compositions were expressed relative to VPDB by reference to in-house carbonate standards calibrated to NBS-19. Reproducibility is ± 0.1‰ for O, and < 0.1‰ for C.

Standard palynological techniques (Wood *et al.*, 1996) were used, and sample preparation was carried out at the National Oceanographic Centre, University of

Southampton, UK. The samples were rough-crushed and then subjected to successive treatments in 30% HCl and 60% HF, with both treatments being followed by rinsing of the sample with deionized water to neutral pH. Following the HF treatment, the samples were sieved at 15 μm. This process was followed by a short treatment in hot concentrated HCl to solubilize any neoformed fluorides. The samples were then diluted with 500 ml of water and sieved again at 15 μm. The resulting kerogen concentrate was stored in vials, and strew-slides were mounted in Elvacite 2044.

Multi-taper (MTM: multi-taper method; 3π) spectral analyses, with robust red noise models (Mann and Lees, 1996), of the obtained integrated Lower Jurassic (Uppermost Rhaetian to Lower Pliensbachian at St Audries Bay, East Quantoxhead and Kilve) $\delta^{13}C_{TOC}$ and TOC record in the time domain (Fig. 5), was performed using the Astrochron (R (3.1.2) Package for astrochronology, version 0.3.1) toolkit (Meyers, 2014), following the short and long eccentricity interpretations as presented in Ruhl *et al.* (2010) and Hüsing *et al.* (2014). Dominant spectral components (Fig. 5) were subsequently filtered from the data series and compared to the data in the time domain, and the interpreted short- and long-eccentricity periodicities (Fig. 6).

[4] RESULTS

[4.1] Early Sinemurian $\delta^{13}C$ and kerogen characterization at Kilve

The TOC content in the studied succession is generally between 1–3%, but increases up to 10.9% in the organic-rich laminated black-shale interval at the lower part of the succession. Total organic-carbon values are also elevated at discrete horizons at ~3, ~6.5, ~10.8 and ~12.9 m in the cliff section at Kilve (Fig. 3). High-resolution carbon-isotope analyses of bulk-rock samples, from ~4 m below the black-shale interval up to 4.5 m above the methane-seep horizon, exhibit a distinct 3‰ negative excursion in $\delta^{13}C_{TOC}$ and a 2‰ negative excursion in $\delta^{13}C_{carb}$ (Fig. 3). The $\delta^{13}C_{TOC}$ negative shift is similar in magnitude to that previously observed in coeval strata of nearby East Quantoxhead (Ruhl *et al*., 2010). The depleted $\delta^{13}C_{TOC}$ directly coincides with elevated TOC values in the laminated black shale; $\delta^{13}C_{carb}$ values remain,

however, low for another ~1.5 m, with TOC concentrations already restored to background values (Fig. 3). Hydrogen Indices from Rock Eval pyrolysis vary between 108 and 720 mg HC/g TOC, with consistently elevated values in the laminated black-shale interval (Fig. 3). Elevated HI values closely match high TOC in the lower part of the section (up to 7 m), but this relationship breaks down in the upper part of the studied interval (Fig. 3). Tmax values of 428–440°C suggest an immature to early mature kerogen in the studied succession (Supplementary Table 1). The characterization of kerogen type, defined by both HI and Tmax values of the studied samples, suggests a gradual transition of kerogen Type II, to Type I and back to Type II/III up-section (Fig. 3). These transitions suggest distinct changes in the composition of the sedimentary organic matter in terms of the relative proportions of marine phytoplankton and terrestrial higher-plant organic matter. The bulk-rock $\delta^{13}C_{carb}$ record of the Lower Sinemurian at Kilve, geographically ~50 m away from the nearest visible conical seep mound (although mounds may be hidden in the cliff near the sampled section), also exhibits a shift to relatively depleted values at the level of the seep mounds (Fig. 3).

[4.2] **$\delta^{13}C$ analyses of Lower Toarcian conical seep mounds at Ravenscar**

The previously published isotopic analyses of bulk-rock samples of the Lower Sinemurian seep mounds at Kilve show relatively depleted values for both carbon and oxygen ($\delta^{13}C_{carb}$: 0 to –32‰; $\delta^{18}O_{carb}$: –3 to –11‰; Fig. 4; Allison *et al*., 2008; Price *et al*., 2008). The isotopic analyses of bulk-rock samples of the Lower Toarcian seep mounds at Ravenscar (Yorkshire, UK) reported here also show relatively depleted values for both carbon and oxygen ($\delta^{13}C_{carb}$: –6 to –18‰; $\delta^{18}O_{carb}$: –10 to –14‰; Fig. 4).

[4.3] **Palynomorph and kerogen assemblages**

Samples studied for palynomorphs and kerogen are generally strongly enriched in amorphous organic matter (AOM), which is typical for black shales, and the palynomorph diversity is relatively low (Fig. 3). The percentage AOM relative to total kerogen (% AOM/total kerogen) is especially high (up to 80%) in the black-shale interval, where wood accounts for only 8%

of the total kerogen (Fig. 3, Supplementary Table 2). Fern spores are generally low in abundance, whereas the gymnosperm pollen species *Classopollis meyeriana* is consistently superabundant, accounting for more than 88% of the total terrestrial palynomorph composition (Fig. 3). The *Classopollis meyeriana* abundance increases to almost 100% of the terrestrial palynomorph fraction in the laminated black-shale interval (Fig. 3). A subsequent change in palynofacies is observed from 6.15 m upwards, where the palynomorph composition becomes more diverse, with the presence of acritarch genus *Micrhystridium*; the amount of wood fragments also increases (Fig. 3; Supplementary Table 2). By contrast, palynomorph diversity is much lower, AOM content is higher, and the prasinophyte (green algae) genus *Tasmanites* dominates the microplankton in the laminated black shale with depleted $\delta^{13}C$ values (Fig. 3; Supplementary Table 2).

The relative abundance of *Tasmanites*, relative to the total microplankton assemblage, gradually decreases from 100% at the top of the laminated black-shale interval to ~16% at the top of the studied section (Fig. 3). The percentage of marine palynomorphs relative to the total palynomorph assemblage (marine + terrestrial palynomorphs) is generally low (< 13.4%), and is especially low in the laminated black-shale interval (Fig. 3).

[5] DISCUSSION

[5.1] The Early Sinemurian $\delta^{13}C$ record, orbital pacing of palaeoclimate and palaeoenvironment

The observed ~3‰ negative excursion in $\delta^{13}C_{TOC}$ at Kilve (Fig. 3) stratigraphically coincides with a similarly sized negative CIE at East Quantoxhead (Fig. 2; Ruhl *et al*., 2010). The contemporaneous ~2‰ negative excursion in $\delta^{13}C_{carb}$ at Kilve (Fig. 3) may reflect changes in the carbon-isotope composition of Early Sinemurian seawater DIC in the Bristol Channel Basin, at a time of basin restriction during sea level lowstand. Combined, these data may suggest a change in the isotopic composition of the globally exchangeable carbon pools. Similarly, the observed sedimentary carbon-isotope fluctuations throughout the earliest Jurassic (Hettangian) in the marine sediments of the Bristol Channel Basin (Hesselbo *et al*.,

2002; Clémence *et al*., 2010; Ruhl *et al.*, 2010), may also have reflected true changes in the global exogenic carbon cycle because carbon-isotope fluctuations equal in magnitude and spacing are also present in the sedimentary organic matter of the continental Newark and Hartford Basin in the eastern USA (Whiteside *et al.*, 2010). Alternatively, periodic changes in the source of the sedimentary organic matter (explaining varying $\delta^{13}C_{TOC}$) and/or periodic changes in the water-column redox state may have taken place, with the oxidation of sedimentary organic matter and the release and subsequent biomineralization of ^{12}C during phases of re-oxygenation (explaining varying $\delta^{13}C_{carb}$) (Clémence *et al.*, 2010; Ruhl *et al.*, 2010).

The $\delta^{13}C_{carb}$ record at Kilve remains low (for another ~1.5 m) following the recovery of the $\delta^{13}C_{TOC}$ signal (Fig. 3). Sedimentary organic-matter content in limestone and mudstone stratigraphically overlying the organic-rich black shales is likely to have been partly reworked and of a mixed marine/terrestrial origin, resulting in somewhat elevated HI values (Fig. 3). The organic-rich laminated black shale was probably deposited under anoxic (or euxinic) conditions, given the distinct lack of bioturbation. By contrast, the underlying and overlying mudrock beds are strongly bioturbated, and the trace fossil *Diplocraterion* reappears at the top of the black-shale interval (Fig. 3). The re-establishment of oxygenated conditions following the deposition of the organic-rich black shale, may have oxidized and remobilized the ^{12}C-enriched organic carbon (Clémence *et al*., 2010). Degradation of the sedimentary organic matter, following the deposition of organic-rich black shale, and the subsequent release of isotopically light (^{12}C-enriched) carbon into the pore-space and overlying seawater DIC pools allowed for the precipitation of isotopically depleted (diagenetic) carbonate. Alternatively, anaerobic oxidation of methane under anoxic/euxinic conditions in the sedimentary pore space during deposition of the organic-rich black shale may have significantly decreased the carbon-isotope composition of interstitial fluids and the overlying water column. Such a process may also have allowed cementation at the seabed or in the shallow subsurface during deposition of the organic-lean mudrocks, following the formation of the organic-rich black shale.

394 Irrespective of the true cause of carbon-isotope changes in the Lower Jurassic
395 sedimentary records of the Bristol Channel Basin, the observed fluctuations in biota,
396 lithology, sedimentary organic matter, TOC and $\delta^{13}C$ are periodic in nature and probably
397 reflect high-frequency climatic and environmental change at Milankovitch periodicities
398 (Bonis *et al.*, 2010; Clémence *et al*., 2010; Ruhl *et al*., 2010; Whiteside *et al.*, 2010; Hüsing *et*
399 *al.*, 2014; Sha *et al.*, 2015). The Lower Sinemurian *C. rotiforme* ammonite Subzone was
400 previously suggested to coincide with a sea-level lowstand (Hesselbo and Jenkyns, 1998).
401 The laminated black shales in the Bristol Channel Basin of *C. rotiforme* ammonite Subzone
402 age, however, formed directly in line with eccentricity modulated, precession-controlled
403 laminated black shales throughout the Hettangian and the Lower Sinemurian, suggesting
404 astronomical control as the dominant factor on the depositional environment rather than sea-
405 level change, although the two mechanisms may not be mutually exclusive (Ruhl *et al*., 2010;
406 Hüsing *et al.*, 2014). The laminated black shale of the *C. rotiforme* Subzone studied here, is,
407 however, arguably stratigraphically more expanded and more organic-rich compared to the
408 underlying Upper Hettangian and Lower Sinemurian strata (Fig. 2).
409 Possible analogues are the TOC-rich Pliocene–Pleistocene sapropels in the Eastern
410 Mediterranean, the periodic development of which was strongly paced by eccentricity
411 modulated precession forcing with the development of anoxic bottom-water conditions in
412 response to regional changes in runoff (Hilgen, 1991; Calvert and Fontugne, 2001; Lourens *et*
413 *al.*, 2004; Becker *et al.*, 2005; Bosmans *et al.*, 2015). In addition, Palaeocene and Eocene
414 hyperthermal events were marked by distinct changes in the global carbon cycle, with major
415 implications for global palaeoclimate and palaeoenvironment,and they, also, were paced at
416 orbital timescales (Lourens *et al.*, 2005; Zachos *et al.*, 2010). The Eocene Thermal Maxima 2
417 and 3 (ETM2 and ETM3) occurred during short- and long-term eccentricity maxima and
418 possibly even at longer (~1.2 Myr) periodicity maxima, whereas the pacing of ETM1 (at the
419 Palaeocene–Eocene boundary) is slightly out of phase, possibly due to non-orbital internal
420 forcing of the Earth system (Zachos *et al.*, 2010).

421 The observed Early Jurassic Hettangian and Sinemurian periodic formation of
422 laminated black shales and coeval fluctuations in $\delta^{13}C$ and palaeoenvironmental proxies (e.g.
423 biological proxies, $CaCO_3$, magnetic susceptibility, TOC) in the Bristol Channel Basin are
424 also paced at orbital time-scales (Figs 2, 5 and 6; Bonis *et al.*, 2010; Clémence *et al.*, 2010;
425 Ruhl *et al*., 2010; Hüsing *et al.*, 2014). These features likely reflect intensified, regional to
426 global, palaeoenvironmental change on short astronomical (precession) timescales, modulated
427 by short- (~100 kyr) and long-term (~405 kyr) (and possibly even longer ~2 Myr) eccentricity
428 (Figs 2 and 6; Ruhl *et al*., 2010; Hüsing *et al.*, 2014; Sha *et al.*, 2015), coeval with
429 eccentricity modulated precession and obliquity forcing in the continental Newark (eastern
430 USA) and Jungar (northwestern China) Basins (Kent and Olsen, 2008; Sha *et al.*, 2015).
431 Periodic palaeoenvironmental and palaeoceanographic changes in the Hettangian and
432 Sinemurian of the Bristol Channel Basin are relatively minor compared with the Triassic–
433 Jurassic boundary and the Early Toarcian oceanographic changes which are both more intense
434 and longer in duration (Suan *et al*., 2008; Deenen *et al.*, 2010; Ruhl *et al.*, 2010; Kemp *et al.*,
435 2011; Huang and Hesselbo, 2014; Boulila *et al*., 2014). Similar to the ETM1 (at the
436 Palaeocene–Eocene boundary), these events were suggested to have resulted from internal (i.e.
437 volcanic) forcing of the Earth system (e.g. Hesselbo *et al.*, 2002; Deenen *et al*., 2010; Jenkyns,
438 2003, 2010; Ruhl *et al.*, 2011; Sell *et al.*, 2014; Percival *et al*., 2015). Studying the time
439 periods between such major events allows for better constraints on the background sensitivity
440 of the Earth system, and our data suggest that major changes in the palaeoenvironment and
441 basin oceanography manifestly occurred on orbital timescales, in a warm, largely ice-free,
442 world.
443
444 [5.2] **Early Sinemurian climatic and environmental change**
445 Elevated TOC contents of up to 10% in the Lower Sinemurian laminated black-shale interval
446 studied here coincide with Type I/II kerogen (high HI values of > 700 mg HC/g TOC) (Fig. 3)
447 and increased amounts of AOM. This Type I kerogen may have been sourced by bacterially
448 degraded marine algal organic matter (Fig. 3). Alternatively, lipid remains of leaf waxes may

449 have been the source of this type of kerogen with high HI values (Wignall, 1994; Tyson,
450 1995; Killops and Killops, 2005). Similarly, the end-Triassic mass-extinction interval in the
451 Eiberg Basin of Austria is marked by strongly enhanced HI values, coinciding with a shift to
452 almost 100% *Classopollis meyeriana* in terms of the total terrestrial palynomorph assemblage
453 (Ruhl *et al*., 2010; Fig. 3).

454 The superabundance of the *Classopollis* pollen, inferred to be a thermophilic taxon
455 during this interval, suggests a shift to even warmer climatic conditions from an already
456 greenhouse state in the Hettangian (Bonis *et al.*, 2010; Bonis and Kurschner, 2012; Riding *et*
457 *al.*, 2013). Possible astronomically controlled changes in the hydrological cycle during this
458 warm phase in the Early Jurassic Hettangian stage, potentially influencing the supply of
459 terrestrial organic matter to the basin, may have significantly affected the marine
460 palaeoenvironment (Bonis *et al.*, 2010). Alternatively, the enhanced supply of terrestrial
461 organic matter may have resulted from an approaching palaeocoastline during an Early
462 Sinemurian sea-level lowstand (Hesselbo and Jenkyns, 1998). The bloom of the *Tasmanites*
463 green algae (a "disaster index") during the Early Sinemurian negative perturbation in $\delta^{13}C$,
464 similar to that following the end-Triassic mass extinction in the Bristol Channel and the west
465 Germanic basins (van de Schootbrugge *et al.*, 2007; Richoz *et al.*, 2012), suggests a salinity-
466 and/or temperature-stressed environment in the marine realm at this time (Vigran *et al.*,
467 2008). The change in the sedimentary organic-matter type, combined with the change in
468 apparent redox state of waters in the Bristol Channel Basin during the studied time interval,
469 could potentially explain the observed changes in the organic and inorganic $\delta^{13}C$ values.
470 Whether the negative CIE is a local (kerogen source-related or diagenetic) phenomenon or
471 represents global carbon-cycle change remains to be tested in other basins or by the sampling
472 of specific carbon pools. The changes in sedimentary geochemistry and organic matter do,
473 however, suggest changes in global climate and the terrestrial and marine palaeoenvironment
474 at orbital timescales.

475

476 [5.3] **Methane seepage linked to organic-rich shale formation**

Marine methane seepage and the formation of authigenic carbonates in/on the seabed have occurred before and throughout the Phanerozoic, in a wide variety of environments and with many different (shallow and deep) sources for the biogenic/thermogenic methane (Tryon *et al.*, 2002; Jiang *et al.*, 2003; Niemann *et al.*, 2006; Walter Anthony *et al.*, 2012; Kiel *et al.*, 2013; Nesbitt *et al.*, 2013; Skarke *et al.*, 2014). One of the best-studied Jurassic methane seeps formed in the Oxfordian time (~160 Ma) at Beauvoisin, southeast France (Peckmann *et al.*, 1999). Highly depleted $\delta^{13}C_{carb}$ values of down to –30‰ in calcite nodules within the Oxfordian section likely result from hydrocarbon-sourced methane seepage (Louis-Schmid *et al.*, 2007).

The conical seep mounds described here now occur ~5 m stratigraphically above the top of the laminated black-shale interval and crop out on the foreshore at Kilve. Previous analyses of these conical mounds indicated that they were likely formed as seafloor mud volcanoes associated with methane seepage (Allison *et al.*, 2008; Price *et al.*, 2008). Micritic carbonate on the flanks of the mounds typically show strongly depleted $\delta^{13}C_{carb}$ values of 0 to –32‰, which likely resulted from microbial anaerobic methanotrophy and subsurface methanogenesis (Allison *et al.*, 2008; Price *et al.*, 2008). The isotopic compositions of coeval mudrocks adjacent to the seep mounds are generally less depleted in $\delta^{13}C_{carb}$, but still display values of down to –20‰ (Allison *et al.*, 2008). The coeval stratigraphical level in the cliff section studied here, ~50 m away from the nearest visible mound on the foreshore, also shows an abrupt shift towards more depleted $\delta^{13}C_{carb}$ values (from +1 to –0.5‰), suggesting that methane seepage from the mud mounds actively altered the isotopic composition of the nearby DIC pool during oxidation of methane at or just below the seabed (Fig. 3; cf. Mediterranean analogue from Aloisi *et al.*, 2000). Alternatively, these values may come from methane diffusion through the sedimentary column and (authigenic) carbonate formation in the sedimentary pore space or at the seabed. The $\delta^{13}C_{TOC}$ record from the same cliff section, however, does not show a coeval shift to more depleted values, and sedimentary organic matter at this stratigraphic interval is terrestrially dominated (with low HI values of 200 mg HC/g TOC and relatively sparse (6%) marine palynomorphs (Fig. 3)). Therefore, methane

505 seepage from the seafloor was likely localized and concentrated at the seep mounds, with its
506 oxidation mostly at and around the mounds and with limited dispersion into the surrounding
507 water-column and atmosphere.

508 The nature and source of fluids released through the early Sinemurian seafloor seeps
509 was previously suggested as resulting from compaction of Triassic pore water (Cornford,
510 2003), or as biogenic methane from the directly underlying organic-rich shale (Allison *et al*.,
511 2008); alternatively the methane may have had a thermogenic origin, being derived from
512 Palaeozoic rocks in the deep subsurface (Price *et al*., 2008). The latter model would suggest a
513 migration of methane gas along deep fault systems to the surface (Cornford, 2003). The seep
514 mounds are, however, randomly located on the foreshore and do not show any clear
515 alignment along the observable fault systems.

516 The model proposed here (Fig. 7) suggests that biogenic methane was sourced from the
517 underlying Lower Sinemurian laminated organic-rich black shale of the *A. bucklandi*
518 ammonite Zone. In this model, organic-lean mudstones from the Lower Sinemurian *A.*
519 *bucklandi* ammonite Zone formed under oxygenated seafloor conditions, due to limited
520 supply of marine and terrestrial organic matter (Phase 1, Fig. 7). Oxygenated conditions in the
521 pore water and minor microbial methanogenesis generated only a minor flux (if any at all) of
522 methane gas across the sediment–water interface and into the overlying water column.
523 Palaeoenvironmental and palaeoceanographic changes in response to orbitally paced changes
524 in climate and palaeoenvironment may have enhanced the hydrological cycle, leading to an
525 increased flux of terrestrial organic matter into the basin (Phase 2, Fig. 7; Fig. 3). Enhanced
526 nutrient supply possibly also initiated increased marine primary productivity. This larger flux
527 of carbon to the sedimentary organic matter pool, in concert with possible density
528 stratification of the water column resulting from increased runoff (Weedon, 1986;
529 Waterhouse, 1999), likely initiated a switch to anoxic conditions in the sedimentary pore
530 water and possibly also the overlying water column. The increased flux of organic carbon,
531 combined with enhanced preservation under anoxic conditions, ultimately resulted in the
532 formation of the laminated organic-rich black shale, with TOC > 10% (Fig. 3). Anoxic

conditions in the sedimentary pore space may have initiated microbial methanogenesis (Niemann *et al.*, 2006) with a strongly enhanced flux of methane to the sediment–water interface, similar to modern-day anoxic/organic-rich lakebeds or in the modern-day Black Sea (Mazzini *et al.*, 2004). Transition back to earlier climatic and environmental conditions returned the system to organic-lean mudrock deposition (Phase 3, Fig. 7; Fig. 3). An elevated flux of biogenic methane from the underlying organic-rich laminated shale, however, still reached the sediment–water interface under conditions of elevated methane pore pressure and an (non-compacted/non-cemented) open pore space in the overlying organic-lean mudrock. Continued burial of the laminated organic-rich shale, possibly with the initiation of compaction and/or cementation of the host rock, may have prohibited biogenic methane from reaching the sediment–water interface via random dispersion through the pore spaces of the overlying mudrock (Phase 4, Fig. 7). Over-pressured free methane in the organic-rich host rock may have migrated upwards by diffusion, possibly along faults that were initiated, for example, due to compaction-related failure (Cornford, 2003; Talukder, 2012). Alternatively, the channelling of free biogenic methane from the organic-rich black shale to the sediment-water interface may have occurred through pipe-conduits, likely resulting in highly localized methane release from the seabed into the overlying water-column, allowing seep mounds to form. Such a model directly explains the observations made within the Lower Sinemurian succession at Kilve.

Interestingly, similar observations were made for the Lower Toarcian succession at Ravenscar, Yorkshire, UK (Hesselbo *et al*., 2013 and herein). Methane-seep carbonates, similarly with depleted $\delta^{13}C_{carb}$ values of –6 to –18‰, occur ~3 m stratigraphically above the most organic-rich interval (up to 19% TOC) in the Lower Toarcian organic-rich Jet Rock (Mulgrave Shale Member; Figs 4 and 8; Hesselbo *et al*., 2013; Kemp *et al.*, 2011). There, the seep occurrences are roughly aligned along the nearby Peak Fault. The sedimentary organic matter in the Jet Rock at Port Mulgrave was dominantly sourced by marine algae deposited under anoxic to euxinic conditions (Salen *et al.*, 2000, French *et al*., 2014). Differences in the stratigraphical distance between the top of the organic-rich black-shale interval and the

561 subsequent occurrence of methane-seep mounds in the Lower Sinemurian of Somerset (~5 m)
562 and the Lower Toarcian of Yorkshire (~3 m), may reflect differences in lithology and original
563 pore space and thus different compaction rates or differences in water depth and/or
564 sedimentary TOC content, potentially leading to differences in the build-up of over-pressure
565 in the sediment pile. Interestingly, conduit like sedimentary carbonate structures do occur in
566 the studied succession, directly preceding the methane seeps, suggesting a direct channelling
567 of free methane from the TOC-rich Jet Rock upwards. With the model proposed here,
568 formation of seabed methane-seep mounds would probably occur in a limited stratigraphical
569 window after the deposition of an organic-rich black shale: after sufficient compaction and
570 the formation of subsurface structures (i.e. faults) for the channelling of free methane, but
571 before complete closure (by compaction or cementation) of the interstitial pore space.
572
573 **[6] CONCLUSIONS**
574 Changes in the isotopic composition of organic and inorganic sedimentary carbon from the
575 Lower Sinemurian (*A. bucklandi* ammonite Zone) sedimentary record at Kilve, Somerset, UK
576 (Bristol Channel Basin) coincided with changes in the depositional environment and
577 palaeoclimate. The 3‰ negative excursion in the $\delta^{13}C_{TOC}$ and the 2‰ negative excursion in
578 the $\delta^{13}C_{carb}$, in concert with a mass bloom of *Tasmanites* (green algae) and an apparent shift to
579 anoxic/euxinic water-column conditions, coincided with the deposition of organic-rich
580 laminated black shales. These phenomena, combined with a change in the terrestrial
581 vegetation assemblage, occurred over a period of ~100 kyr. This perturbation of the
582 palaeoenvironment was in phase with a long-term (~405 kyr) eccentricity maximum and
583 succeeds similar, but less intense, events throughout the Early Jurassic Hettangian Stage in
584 the Bristol Channel Basin.
585 The formation of methane-seep mounds on the Early Sinemurian (*A. bucklandi*
586 ammonite Zone) seabed in the Kilve area followed the deposition of organic-rich laminated
587 black shale deposition by ~200 kyr (~5 m). Seep formation possibly resulted from biogenic
588 methane production (by microbial methanogenesis) in the organic-rich shale and the

589 channelling of this gas, which was likely over-pressured in the pore spaces of the source-rock,
590 along fractures and faults to the sediment–water interface. Similar observations, with
591 methane-seep mounds forming stratigraphically closely above the Lower Toarcian organic-
592 rich Jet Rock at Ravenscar, Yorkshire, UK, suggests that seabed seep mound formation could
593 be a common phenomenon in the stratigraphical record, following local, regional or global
594 black-shale deposition.
595
596 **ACKNOWLEDGEMENTS**
597 Shell International Exploration & Production B.V. is acknowledged for funding of this project.
598 James B. Riding publishes with the approval of the Executive Director, British Geological
599 Survey (NERC). We thank Peter Ditchfield and Steve Wyatt (Oxford University), and Mabs
600 Gilmour and Simona Nicoara (Open University) for carbon-isotope analyses and help in the
601 laboratory. John Marshall (University of Southampton) is thanked for palynological
602 preparations. We are grateful to David Kemp and Helmut Weissert for their constructive
603 reviews and to Editor Maria Rose Petrizzo for her constructive review and helpful summary
604 comments, which significantly improved this manuscript.
605
606 **FIGURE CAPTIONS**
607 **Fig. 1.** Geographical maps. (A) Early Jurassic global palaeogeography, modified after Dera *et*
608 *al*. (2011) and Korte *et al.* (2015). (B) Zoom-in map of the red-square-marked area in map A,
609 showing the palaeogeographic position (red stars) of the Bristol Channel Basin (with the
610 Kilve section) and the Cleveland Basin (with the Ravenscar, Hawsker Bottoms and Staithes
611 sections) at the northwestern end of the Tethys Ocean; (C) Map of the present-day Bristol
612 Channel with sample localities marked (modified after Ruhl *et al.*, 2010).
613 **Fig. 2.** Upper Triassic and Lower Jurassic (Hettangian and Early Sinemurian) $\delta^{13}C_{TOC}$ and
614 TOC data from the Bristol Channel Basin sections at St Audries Bay and East Quantoxhead
615 (Hesselbo *et al.*, 2002, Ruhl *et al.*, 2010; Hüsing *et al.*, 2014) showing a pronounced ~3‰

616 negative shift in $\delta^{13}C_{TOC}$ in the Lower Sinemurian *A. bucklandi* ammonite Zone.
617 Palaeomagnetic data from Hounslow *et al.* (2004) and Hüsing *et al.* (2014). $\delta^{13}C_{TOC}$ and
618 $\delta^{13}C_{carb}$ data from the Bristol Channel Basin at Kilve (this study) show a similar ~2–3‰
619 negative excursion in coeval strata from East Quantoxhead. The dark-grey-coloured band
620 represents the TOC-rich laminated black-shale horizon as in Figure 6. The blue-coloured band
621 represents the stratigraphic level of methane-seep mounds at the Lower Sinemurian foreshore
622 outcrop at Kilve.

623 **Fig. 3.** Sedimentary description and geochemical and palynological results from the *A.*
624 *bucklandi* ammonite zone of Kilve, Somerset, UK. Geochemical data, including $\delta^{13}C_{TOC}$,
625 $\delta^{13}C_{carb}$, TOC and HI are in black and grey squares. Palynological results including (%
626 *Classopollis meyeriana*) / (total terrestrial palynomorphs), (% *Tasmanites* spp.) / (total
627 microplankton), (% marine palynomorphs) / (total marine + terrestrial) and (% AOM) / (total
628 kerogen) are in black circles (AOM = amorphous organic matter). Levels of methane seepage
629 and organic-rich black-shale occurrence are marked by, respectively, blue and grey bands. A
630 pseudo-Van Krevelen diagram (with HI *vs* Tmax) is given on the left (following Delvaux *et*
631 *al*., 1990), with red squares representing samples from the level of the negative carbon-
632 isotope excursion (CIE).

633 **Fig. 4.** Outcrop and methane-seep mound images and associated geochemical data from Kilve
634 (Somerset, UK) and Ravenscar (Yorkshire, UK). Photographs (A), (B), (C) and (D) show
635 methane-seep mounds from Kilve. Photograph (E) shows a methane-seep mound from
636 Ravenscar. In the cross-plots between $\delta^{13}C_{carb}$ and $\delta^{18}O_{carb}$, red circles represent values from
637 the Early Sinemurian methane-seep mounds at Kilve (Allison *et al*., 2008; Price *et al*., 2008)
638 and the Early Toarcian methane-seep mounds at Ravenscar (this study); dark grey squares
639 represent values for the Lower Sinemurian mudrocks in the Kilve cliff-section, ~50 m away
640 from the nearest visible seep mound (this study); dark grey squares also represent values of
641 Lower Toarcian belemnites from Yorkshire (McArthur *et al*., 2000); light grey diamonds
642 represent values from Lower Sinemurian mudrocks at Kilve, which formed stratigraphically

643 above and below the methane-seep mounds (Allison *et al*., 2008); pink triangles represent
644 values from mudrock samples from the mound-bearing bed, in close proximity (1–20 m) to
645 the seep mounds (Price *et al*., 2008). Photograph (F) illustrates the sampled outcrop
646 succession with black-shale interval and methane-seep level marked in yellow and blue.

647 **Fig. 5.** Multi-taper (MTM; 3π) power spectra of the obtained $\delta^{13}C_{TOC}$ and TOC time series
648 (after Ruhl *et al.* (2010) and Hüsing *et al.* (2014)) using the Astrochron (R (3.1.2) Package for
649 astrochronology, version 0.3.1) toolkit (Meyers, 2014), with robust red-noise models (Mann
650 and Lees, 1996). A) $\delta^{13}C_{TOC}$ time-series multi-taper power spectrum of the complete data-set
651 as in Figure 6, showing dominant short ~100 kyr eccentricity and long 2–2.4 myr
652 astronomical forcing. B) Multi-taper power spectrum of the high-frequency (0–0.8 Myr)
653 band-pass filter of the $\delta^{13}C_{TOC}$ time-series, showing dominant short (~100 kyr) and long (~405
654 kyr) eccentricity. C) TOC time-series multi-taper power spectrum of the complete dataset (as
655 presented in Figure 6), showing dominant short (~100 kyr) eccentricity and long 405 kyr to
656 2–2.4 myr astronomical forcing. $\delta^{13}C_{TOC}$ and TOC time-series data were first manipulated to
657 give uniform sample spacing using linear interpolation. MTM power estimates, AR1
658 confidence-level estimates and harmonic test confidence-level estimates are also performed
659 with Astrochron. An independent check of the dominant spectral components has been
660 performed with AnalySeries 2.0.8 (Paillard *et al.*, 1996), giving an 80% confidence interval
661 (grey).

662 **Fig. 6.** Upper Triassic to Lower Jurassic (Uppermost Rhaetian to Lower Sinemurian) $\delta^{13}C_{TOC}$
663 and total organic carbon (TOC) composite from the Westbury, Lilstock and Blue Lias
664 Formation at St Audries Bay (Hesselbo *et al.*, 2002; Ruhl *et al.*, 2010), East Quantoxhead
665 (Ruhl *et al.*, 2010; Hüsing *et al.*, 2014) and Kilve (Somerset, UK) (this study), plotted against
666 numerical (absolute) time following bio-, magneto- and cyclostratigraphic and radiometric
667 correlation between the Bristol Channel Basin (UK; this study; Hesselbo *et al.*, 2002;
668 Hounslow *et al*., 2004; Ruhl *et al.*, 2010; Hüsing *et al.*, 2014), the Newark and Hartford
669 Basins (USA; Kent and Olsen, 2008; Blackburn *et al.*, 2013), the Fundy Basin (Canada;

Schoene *et al.,* 2010), the Pucara Basin (Peru; Sell *et al.*, 2014), New York Canyon (Nevada, USA; Schoene *et al.,* 2010) and the La2010$^{a/b/c/d}$ astronomical solutions (Laskar *et al.*, 2011). Radiometric age-constraints are from [A: Schaltegger *et al*., 2008; Guex *et al*., 2012], [B: Guex *et al*., 2012], [C: Guex *et al*., 2012], [D: Schoene *et al*., 2010; Guex *et al*., 2012], [E: Schoene *et al*., 2010; Guex *et al*., 2012], [F: Schaltegger *et al*., 2008; Schoene *et al*., 2010; Guex *et al*., 2012], [G: Guex *et al*., 2012], [H: Blackburn *et al.*, 2013] and [I: Schoene *et al*., 2010].

Fig. 7. A suggested model explaining subsequent phases of change in the environmental and depositional environment leading to methane-seep mound formation, sourced by shallow-subsurface biogenic methane. Phase 1: the formation of organic-lean mudstones under oxygenated seafloor conditions with minor microbial methanogenesis generated only a minor flux (if any at all) of methane gas across the sediment–water interface and into the overlying water column; Phase 2: organic-rich laminated black shale deposited under anoxic conditions with microbial methanogenesis causing a strongly enhanced flux of methane to the sediment–water interface; Phase 3: transition back to organic-lean mudstone deposition under oxic conditions with still elevated flux of biogenic methane from the underlying organic-rich laminated shale reaching the sediment–water interface under conditions of elevated methane pore pressure and a (non-compacted/non-cemented) open pore space in the overlying organic-lean mudrock; Phase 4: continued burial of the laminated organic-rich shale, possibly with the initiation of compaction and/or cementation of the host rock, potentially prohibited biogenic methane from reaching the sediment–water interface via random dispersion through the pore spaces of the overlying mudrock. Channeling of methane resulted in the localized transfer of methane across the sediment-water interface and the formation/deposition of (authigenic) carbonates and carbonaceous methane seeps.

Fig. 8. Lithostratigraphy of the Lower Sinemurian in the Bristol Channel Basin at the Kilve section (Somerset, UK) and the Lower Toarcian in the Cleveland Basin at the Ravenscar section (Yorkshire, UK). The methane seeps at Kilve appear at one horizon marked by the

blue coloured band; methane associated carbonate concretions and conduits at Ravernscar occurred sporadically throughout the marked interval adjacent to the Peak Fault. In both localities, the seeps and conduits occur stratigraphically above the intervals of laminated organic-rich black shale marked by the grey band. TOC records are from this study (Kilve) and Kemp *et al*. (2011) (Yorkshire).

REFERENCES

Al-Suwaidi, A.H., Angelozzi, G.N., Baudin, F., Damborenea, S.E., Hesselbo, S.P., Jenkyns, H.C., Mancenido, M.O. and **Riccardi, A.C.** (2010) First record of the Early Toarcian Oceanic Anoxic Event from the Southern Hemisphere, Neuquén Basin, Argentina. *J. Geol. Soc. London*, **167**, 633–636.

Al-Suwaidi, A.H., Hesselbo, S.P., Damborenea, S.E., Manceñido, M.O., Jenkyns, H.C., Riccardi, A.C., Angelozzi, G.N. and **Baudin, F**. (2016) The Toarcian Oceanic Anoxic Event (Early Jurassic) in the Neuquén Basin, Argentina: A Reassessment of Age and Carbon Isotope Stratigraphy. *J. Geol.*, **124**, 171–193.

Allison, P.A., Hesselbo, S.P. and **Brett, C.E.** (2008) Methane seeps on an Early Jurassic dysoxic seafloor. *Palaeogeogr. Palaeoclimatol. Palaeoecol.*, **270**, 230–238.

Aloisi, G., Pierre, C., Rouchy, J.-M., Foucher, J.-P., Woodside, J. and **the MEDINAUT Scientific Party** (2000) Methane-related authigenic carbonates of eastern Mediterranean Sea mud volcanoes and their possible relation to gas hydrate destabilisation. *Earth and Planet. Sci. Lett.*, **184**, 321–338.

Becker, J., Lourens, L.J., Hilgen, F.J., van der Laan, E., Kouwenhoven, T.J. and **Reichart, G.-J.** (2005) Late Pliocene climate variability on Milankovitch to millennialtime scales: A high-resolution study of MIS100 from the Mediterranean. *Palaeogeogr. Palaeoclimatol. Palaeoecol.,* **228**, 338–360.

Behar, F., Beaumont, V. and **De B. Penteado, H.L.** (2001) Rock-Eval 6 Technology: Performances and Developments. *Oil & Gas Science and Technology–Rev. IFP* **56**, 111–134.

Blackburn, T.J., Olsen, P.E., Bowring, S.A., Mclean, N.M., Kent, D.V., Puffer, J., McHone, G., Rasbury, E.T. and **Et-Touhami, M.** (2013) Zircon U-Pb Geochronology Links the End-Triassic Extinction with the Central Atlantic Magmatic Province. *Science*, **340**, 941–945.

Bonis, N.R., Ruhl, M. and **Kürschner, W.M.** (2010) Milankovitch-scale palynological turnover across the Triassic–Jurassic transition at St. Audrie's Bay, SW UK. *J. Geol. Soc.*, **167**, 877–888.

Bonis, N.R. and **Kürschner, W.M.** (2012) Vegetation history, diversity patterns, and climate change across the Triassic/Jurassic boundary. *Paleobiology*, **38**, 240–264.

Bosmans, J.H.C., Drijfhout, S.S., Tuenter, E., Hilgen, F.J., Lourens, L.J. and **Rohling, E.J.** (2015) Precession and obliquity forcing of the freshwater budget over the Mediterranean. *Quat. Sci. Rev.,* **123**, 16–30.

Bottrell, S. and **Raiswell, R.** (1989) Primary versus diagenetic origin of Blue Lias rhythms (Dorset, UK): evidence from sulphur geochemistry. *Terra Nova*, **1**, 451–456.

Boulila, S., Galbrun, B., Huret, E., Hinnov, L. A., Rouget, I., Gardin, S. and **Bartolini, A.** (2014) Astronomical calibration of the Toarcian Stage: Implications for sequence stratigraphy and duration of the early Toarcian OAE. *Earth and Planet. Sci. Lett.*, **386**, 98–111.

Brazier, J., Suan, G., Tacail, T., Simon, L., Martin, J.E., Mattioli, E. and **Balter, V.** (2015) Calcium isotope evidence for dramatic increase of continental weathering during the Toarcian oceanic anoxic event (Early Jurassic). *Earth and Planet. Sci. Lett.*, **411**, 164–176.

Calvert, S.E. and **Fontugne, M.R.** (2001) On the late Pleistocene–Holocene sapropel record of climatic and oceanographic variability in the eastern Mediterranean. *Paleoceanography*, **16**, 78–94.

Campos, H.S. and **Hallam, A.** (1979) Diagenesis of English Lower Jurassic limestones as inferred from oxygen and carbon isotope analysis. *Earth Planet. Sci. Lett.*, **45**, 23–31.

Clémence M.-E., Bartolini A., Gardin S., Paris G., Beaumont V. and **Page K.N. (**2010) Early Hettangian benthic–planktonic coupling at Doniford (SW England): Palaeoenvironmental implications for the aftermath of the end-Triassic crisis. *Palaeogeogr. Palaeoclimatol. Palaeoecol.*, **295**, 102–115.

Cornford, C. (2003) Triassic palaeo-pressure and Liassic mud volcanoes near Kilve, West Somerset. *Geoscience in south-west England*, **10**, 430–434.

Cox, B.M., Stumbler, M.G. and **Ivimey-Cook, H.C.** (1999) A formational framework for the Lower Jurassic of England and Wales (onshore area). *British Geological Survey Research Report*, **RR/99/01**, 1–30.

Deconinck, J.-F., Hesselbo, S.P., Debuisser, N., Averbuch, O., Baudin, F. and **Bessa, J.** (2003) Environmental controls on clay mineralogy of an Early Jurassic mudrock (Blue Lias Formation, southern England). *Int. J. Earth Sci. (Geol Rundsch)*, **92**, 255–266.

Deenen, M.H.L., Ruhl, M., Bonis, N.R., Krijgsman, W., Kuerschner, W.H., Reitsma, M. and **van Bergen, M.J.** (2010) A new chronology for the end-Triassic mass extinction. *Earth Planet. Sci. Lett.*, **291**, 113–125.

Delvaux, D., Martin, H., Leplat, P. and **Paulet, J.** (1990) Geochemical characterization of sedimentary organic matter by means of pyrolysis kinetic parameters. *Org. Geochem.*, **16**, 175–187.

Dera, G., Brigaud, B., Monna, F., Laffont, R., Pucéat, E., Deconinck, J.-F., Pellenard, P., Joachimski, M.M. and **Durlet, C.** (2011) Climatic ups and downs in a disturbed Jurassic world. *Geology*, **39**, 215–218.

Duarte, L.V., Comas-Rengifo, M.J., Silva, R.L., Paredes, R. and **Goy, A.** (2014) Carbon isotope stratigraphy and ammonite biochronostratigraphy across the Sinemurian Pliensbachian boundary in the western Iberian margin. *Bull. Geosciences*, **89**, 719–736.

Duncan, R.A., Hooper, P.R., Rehacek, J., Marsh, J.S. and **Duncan, A.R.** (1997) The timing and duration of the Karoo igneous event, southern Gondwana. *J. Geophys. Res.*, **102**, 18127–18138.

French, K.L., Sepúlveda, J., Trabucho-Alexandre, J., Gröcke, D.R. and **Summons, R.E.** (2014) Organic geochemistry of the early Toarcian oceanic anoxic event in Hawsker Bottoms, Yorkshire, England. *Earth and Planet. Sci. Lett.*, **390**, 116–127.

Gallois, R.W. (1979) Oil Shale Resources in Great Britain. *Institute of Geological Sciences Commissioned Report*, 158 p.

Guex, J., Schoene, B., Bartolini, A., Spangenberg, J., Schaltegger, U., O'Dogherty, L., Taylor, D., Bucher, H. and **Atudorei, V.** (2012) Geochronological constraints on post-extinction recovery of the ammonoids and carbon cycle perturbations during the Early Jurassic. *Palaeogeogr. Palaeoclimatol. Palaeoecol.*, **346–347**, 1–11.

Hallam, A. (1964) Origin of the limestone-shale rhythm in the Blue Lias of England: a composite theory. *J. Geol.*, **72,** 157–169.

Hallam, A. (1986) Origin of minor limestone–shale cycles: climatically induced or diagenetic? *Geology*, **14**, 609–6012.

Hallam, A. (1987) Radiations and extinctions in relation to environmental change in the Marine Lower Jurassic of Northwest Europe. *Paleobiology*, **13**, 152–168.

Hallam, A. (1995) Oxygen-restricted facies of the basal Jurassic of north-west Europe. *Hist. Biol.*, **10**, 247–257.

Hallam, A. (1997) Estimates of the amount and rate of sea-level change across the Rhaetian–Hettangian and Pliensbachian–Toarcian boundaries (latest Triassic to early Jurassic). *J. Geol. Soc. London*, **154**, 773-779.

Hermoso, M., Callonnec, L.L., Minoletti, F., Renard, M. and **Hesselbo, S.P.** (2009) Expression of the Early Toarcian negative carbon-isotope excursion in separated carbonate microfractions (Jurassic, Paris Basin). *Earth and Planet. Sci. Lett.*, **277**, 194–203.

Hesselbo, S.P. and **Jenkyns, H.C.** (1998) Sequence stratigraphy of the Lower Jurassic of the British Isles. In: Mesozoic and Cenozoic Sequence Stratigraphy of Europe (Eds P.-C. de Graciansky, J. Hardenbol, T. Jaquin, P.R. Vail and M.B. Farley). *Spec. Publ. Soc. econ. Paleont. Miner.*, **60**, 561–581.

Hesselbo, S. P. and **Coe, A. L.** (2000). Jurassic sequences of the Hebrides Basin, Isle of Skye, Scotland. In: *Field Trip Guidebook* (Eds J.R. Graham and A. Ryan), International Association of Sedimentologists, Dublin, pp. 41–58.

Hesselbo, S.P., Grocke, D.R., Jenkyns, H.C., Bjerrum, C.J., Farrimond, P., Bell, H.S.M. and **Green, O.R.** (2000) Massive dissociation of gas hydrate during a Jurassic oceanic anoxic event. *Nature*, **406**, 392–395.

Hesselbo, S.P., Robinson, S.A., Surlyk, F. and **Piasecki, S.** (2002) Terrestrial and marine extinction at the Triassic–Jurassic boundary synchronized with major carbon-cycle perturbation: a link to initiation of massive volcanism? *Geology*, **30**, 251–254.

Hesselbo, S.P., Jenkyns, H.C., Duarte, L.V. and **Oliveira, L.C.V.** (2007) Carbon-isotope record of the Early Jurassic (Toarcian) Oceanic Anoxic Event from fossil wood and marine carbonate (Lusitanian Basin, Portugal). *Earth and Planet. Sci. Lett.*, **253**, 455–470.

Hesselbo, S.P. (2008) Sequence stratigraphy and inferred relative sea-level change from the onshore British Jurassic. *Proc. Geol. Assoc.*, **119**, 19–34.

Hesselbo, S.P., Bjerrum, C.J., Hinnov, L.A., MacNiocaill, C., Miller, K.G., Riding, J.B., van de Schootbrugge, B. and **the Mochras Revisited Science Team** (2013) Mochras borehole revisited: a new global standard for Early Jurassic earth history. *Sci. Dril.*, **16**, 81–91.

Hilgen, F.J. (1991) Astronomical calibration of Gaus to Matuyama sapropels in the Mediterranean and implication for the Geomagnetic Polarity Time Scale. *Earth and Planet. Sci. Lett*., **104**, 226–244.

Hounslow, M.W., Posen, P.E. and **Warrington, G.** (2004) Magnetostratigraphy and biostratigraphy of the upper Triassic and lowermost Jurassic succession, St Audrie's Bay, UK. *Palaeogeogr. Palaeoclimatol. Palaeoecol.*, **213**, 331–358.

Huang, C. and **Hesselbo, S.P.** (2014) Pacing of the Toarcian Oceanic Anoxic Event (Early Jurassic) from astronomical correlation of marine sections. *Gondwana Research*, **25**, 1348–1356.

Hüsing SK., Beniest A., van der Boon A., Albels H.A., Deenen M.H.L., Ruhl M. and **Krijgsman W.** (2014) Astronomically-calibrated magnetostratigraphy of the Lower Jurassic marine successions at St. Audrie's Bay and East Quantoxhead (Hettangian–Sinemurian; Somerset, UK). *Palaeogeogr. Palaeoclimatol. Palaeoecol.*, **403**, 43–56.

Jenkyns, H.C. (1985) The Early Toarcian and Cenomanian-Turonian anoxic events in Europe: comparisons and contrasts. *Int. J. Earth Sci.*, **74**, 505–518.

Jenkyns, H.C. (1988). The early Toarcian (Jurassic) anoxic event: Stratigraphic, sedimentary, and geochemical evidence. *Am. J. Sci.,* **288**, 101–151.

Jenkyns, H.C., Jones, C.E., Grocke, D.R., Hesselbo, S.P. and **Parkinson, D.N.** (2002) Chemostratigraphy of the Jurassic System: applications, limitations and implications for palaeoceanography. *J. Geol. Soc. London*, **159**, 351–378.

Jenkyns, H.C. (2003) Evidence for rapid climate change in the Mesozoic–Paleogene greenhouse world. *Phil. Trans. R. Soc. London, Series A*, **361**, 1885–1916.

Jenkyns, H.C. (2010) Geochemistry of oceanic anoxic events. *Geochem. Geophys. Geosyst.*, **11**, Q03004, doi: 10.1029/2009GC002788.

Jenkyns, H.C. and **Weedon, G.P. (**2013) Chemostratigraphy ($CaCO_3$, TOC, $\delta^{13}C_{org}$) of Sinemurian (Lower Jurassic) black shales from the Wessex Basin, Dorset and palaeoenvironmental implications. *Newsletters on Stratigraphy*, **46**, 1–21.

Jiang, G., Kennedy, M.J. and **Christie-Blick, N.** (2003) Stable isotopic evidence for methane seeps in Neoproterozoic postglacial cap carbonates. *Nature*, **426**, 822–826.

Kemp, D.B., Coe, A.L., Cohen, A.S. and **Schwark, L.** (2005) Astronomical pacing of methane release in the Early Jurassic period. *Nature*, **437**, 396–399.

Kemp, D.B., Coe, A.L., Cohen, A.S. and **Weedon, G.P.** (2011) Astronomical forcing and chronology of the early Toarcian (Early Jurassic) oceanic event in Yorkshire, UK. *Paleoceanography*, **26**, PA4210, doi: 10.1029/2011PA002122.

Kent. D.V. and **Olsen, P.E.** (2008) Early Jurassic magnetostratigraphy and paleolatitudes from the Hartford continental rift basin (eastern North America): Testing for polarity bias and abrupt polar wander in association with the central Atlantic magmatic province. *J. Geophys. Res.*, **113**, B06105, doi: 10.1029/2007JB005407.

Kiel, S., Birgel, D., Campbell, K.A., Crampton, J.S., Schioler, P. and **Peckmann, J.** (2013) Cretaceous methane-seep deposits from New Zealand and their fauna. *Palaeogeogr. Palaeoclimatol. Palaeoecol.,* **390**, 17–34.

Killops, S. and **Killops, V. (2005)** Introduction to Organic Geochemistry, *2nd Edition*. Blackwell Publishing, Oxford.

Korte, C., Hesselbo, S.P., Jenkyns, H.C., Rickaby, R.E.M. and **Spotl, C.** (2009) Palaeoenvironmental significance of carbon- and oxygen-isotope stratigraphy of marine Triassic–Jurassic boundary sections in SW Britain. *J. Geol. Soc.*, **166**, 431–445.

Korte, C. and **Hesselbo, S.P.** (2011) Shallow-marine carbon- and oxygen-isotope and elemental records indicate icehouse-greenhouse cycles during the Early Jurassic. *Paleoceanography*, **26**, PA4219, doi: 10.1029/2011PA002160.

Korte, C., Hesselbo, S.P., Ullmann, C.V., Dietl, G., Ruhl, M., Schweigert, G. and **Thibault, N.** (2015) Jurassic climate mode governed by ocean gateway. *Nat. Commun.*, 6:10015, doi: 10.1038/ncomms10015.

Laskar, J., Fienga, A., Gastineau, M. and **Manche, H.** (2011) La2010: a new orbital solution for the long-term motion of the Earth. *A & A*, **532**, A89.

Liang, H., Chen, X., Wang C., Zhao, D. and **Weissert, H.** (2016) Methane-derived authigenic carbonates of mid-Cretaceous age in southern Tibet: Types of carbonate concretions, carbon sources, and formation processes. *J. Asian Earth Sci.*, **115**, 153–169.

Littler, K., Hesselbo, S.P. and **Jenkyns, H.C.** (2010) A carbon-isotope perturbation at the Pliensbachian–Toarcian boundary: evidence from the Lias Group, NE England. *Geol. Mag.,* **147**, 181–192.

Louis-Schmid, B., Rais, P., Logvinovich, D., Bernasconi, S.M. and **Weissert, H.** (2007) Impact of methane seeps on the local carbon-isotope record: a case study from a Late Jurassic hemipelagic section. *Terra Nova*, **19**, 259–265.

Hilgen, F.J., Lourens, L.J. and **Van Dam, J.A.** (2004) The Neogene Period. In: A Geological Timescale 2004. (Eds F. Gradstein, I. Ogg, and A. Smith), pp. 923–978. Cambridge University Press, Cambridge, UK.

Lourens, J.L., Sluijs, A., Kroon, D., Zachos, J.C., Thomas, E., Röhl, U., Bowles, J. and **Raffi, I.** (2005) Astronomical pacing of late Palaeocene to early Eocene global warming events. *Nature*, **435**, 1083–1087.

Mander, L. and **Twitchett, R.J.** (2008) Quality of the Triassic–Jurassic bivalve fossil record in north-west Europe. *Palaeontology*, **51**, 1213–1223.

Mann, M.E. and **Lees, J.M.** (1996) Robust estimation of background noise and signal detection in climatic time series. *Climatic Change*, **33**, 409–445.

Mazzini, A., Ivanov, M.K., Parnell, J., Stadnits, A., Cronin, B.T., Poludetkina, E., Mazurenko, L. and **van Weering, T.C.E.** (2004) Methane-related authigenic carbonates from the Black Sea: geochemical characterisation and relation to seeping fluids. *Marine Geology*, **212**, 153–181.

McArthur, J.M., Donovan, D.T., Thirlwall, M.F., Fouke, B.W. and **Mattey, D.** (2000) Strontium isotope profile of the Early Toarcian (Jurassic) oceanic anoxic event, the duration of ammonite biozones and belemnite palaeotemperatures. *Earth and Planet. Sci. Lett.*, **179**, 269–285.

McElwain, J.C., Wade-Murphy, J. and **Hesselbo, S.P.** (2005). Changes in carbon dioxide during an oceanic anoxic event linked to intrusion into Gondwana coals. *Nature*, **435**, 479–482.

McRoberts, C.A. and **Newton, C.R.** (1995) Selective extinction among end-Triassic European bivalves. *Geology*, **23**, 102–104.

Meyers, S.R. (2014) Astrochron: An R Package for Astrochronology (Version 0.3.1). http://cran.r-project.org/package=astrochron.

Nesbitt, E.A., Martin, R.A. and **Campbell, K.A.** (2013) New records of Oligocene diffuse hydrocarbon seeps, northern Cascadia margin. *Palaeogeogr. Palaeoclimatol. Palaeoecol.*, **390**, 116–129.

Niemann, H., Duarte, J., Hensen, C., Omoregie, E., Magalhães, V.H., Elvert, M., Pinheiro, L.M., Kopf, A. and **Boetius, A.** (2006) Microbial methane turnover at mud volcanoes of the Gulf of Cadiz. *Geochim. Cosmochim. Acta.*, **70**, 5336–5355.

Paillard, D., Labeyrie, L. and **Yiou, P.** (1996) Macintosh program performs time-series analysis, *Eos Trans. AGU*, **77**, 379.

Palmer, C.P. (1972) The Lower Lias (Lower Jurassic) between Watchet and Lilstock in North Somerset (United Kingdom). *Newsletters on Stratigraphy*, **2**, 1–30.

Paul, C.R.C., Allison, P.A. and **Brett, C.E.** (2008) The occurrence and preservation of ammonites in the Blue Lias Formation (lower Jurassic) of Devon and Dorset, England and their palaeoecological, sedimentological and diagenetic significance. *Palaeogeogr. Palaeoclimatol. Palaeoecol.*, **270**, 258–272.

Peckmann, J., Thiel, V., Michaelis, W., Clari, P., Gaillard, C., Martire, L. and **Reitner, J.** (1999) Cold seep deposits of Beauvoisin (Oxfordian; southeastern France) and Marmorito (Miocene; northern Italy): microbially induced authigenic carbonates. *Int. Journ. Earth Sciences*, **88**, 60–75.

Percival, L.M.E., Witt, M.L.I., Mather, T.A., Hermoso, M., Jenkyns, H.C., Hesselbo, S.P., Al-Suwaidi, A.H., Storm, M.S., Xu, W. and **Ruhl, M.** (2015) Globally enhanced mercury deposition during the end-Pliensbachian extinction and Toarcian OAE: A link to the Karoo–Ferrar Large Igneous Province. *Earth and Planet. Sci. Lett.*, **428**, 267–280.

Porter, S.J., Smith, P.L., Caruthers, A.H., Hou, P., Gröcke, D.R. and **Selby, D.** (2014) New high resolution geochemistry of Lower Jurassic marine sections in western North America: A global positive carbon isotope excursion in the Sinemurian?. *Earth and Planet. Sci. Lett.*, **397**, 19–31.

Price, G.D., Vowles-Sheridan, N. and **Anderson, M.W.** (2008) Lower Jurassic mud volcanoes and methane, Kilve, Somerset, UK. *Proc. Geol. Assoc.*, **119**, 193–201.

Richardson, L. (1911) The Rhaetic and contiguous deposits of West, Mid, and part of East Somerset. *Q. J. Geol. Soc. London*, **67**, 1–74.

Richoz, S., van de Schootbrugge, B., Pross, J., Püttmann, W., Quan, T.M., Lindström, S., Heunisch, C., Fiebig, J., Maquil, R. Schouten, S., Hauzenberger, C.A. and **Wignall, P.B.** (2012) Hydrogen sulphide poisoning of shallow seas following the end-Triassic extinction. *Nat. Geosci.*, **5**, 662–667.

Riding, J.B., Leng, M.J., Kender, S., Hesselbo, S.P. and **Feist-Burkhardt, S.** (2013) Isotopic and palynological evidence for a new Early Jurassic environmental perturbation. *Palaeogeogr. Palaeoclimatol. Palaeoecol.*, **374**, 16–27.

Ruhl, M., Deenen, M.H.L., Abels, H.A., Bonis, N.R., Krijgsman, W. and **Kürschner, W.M.** (2010) Astronomical constraints on the duration of the early Jurassic Hettangian

stage and recovery rates following the end-Triassic mass extinction (St Audrie's Bay/East Quantoxhead, UK). *Earth and Planet. Sci. Lett.*, **295**, 262–276.

Ruhl, M., Bonis, N.R., Reichart, G-J, Sinninghe Damsté, J.S. and **Kürschner, W.M.** (2011) Atmospheric Carbon Injection Linked to End-Triassic Mass Extinction. *Science*, **333**, 430–434.

Sælen, G., Tyson, R.V., Telnæs, N. and **Talbot, M.R.** (2000) Contrasting watermass conditions during deposition of the Whitby Mudstone (Lower Jurassic) and Kimmeridge Clay (Upper Jurassic) formations, UK. *Palaeogeogr. Palaeoclimatol. Palaeoecol.*, **163**, 163–196.

Schaltegger, U., Guex, J., Bartolini, A., Schoene, B. and **Ovtcharova, M.** (2008) Precise U–Pb age constraints for end-Triassic mass extinction, its correlation to volcanism and Hettangian post-extinction recovery. *Earth Planet. Sci. Lett.*, **267**, 266–275.

Schoene, B., Guex, J., Bartolini, A., Schaltegger, U. and **Blackburn, T.J.** (2010) Correlating the end-Triassic mass extinction and flood basalt volcanism at the 100 ka level. *Geology*, **38**, 387–390.

Schouten, S., van Kaam-Peters, H.M.E., Rijpstra, W.I.C., Schoell, M. and **Sinninghe-Damsté, J.S.** (2000). Effects of an Oceanic Anoxic Event on the Stable carbon isotopic composition of Early Toarcian Carbon. *Am. J. Sci.*, **300**, 1–22.

Sell, B., Ovtcharova, M., Guex, J., Bartolini, A., Jourdan, F., Spangenberg, J.E., Vicente, J. and **Schaltegger, U. (**2014) Evaluating the temporal link between the Karoo LIP and climatic–biologic events of the Toarcian Stage with high-precision U-Pb geochronology. *Earth and Planet. Sci. Lett.*, **408**, 48–56.

Sha, J., Olsen, P.E., Pan, Y., Xu, D., Wang, Y., Zhang, X., Yao, X. and **Vajda, V.** (2015) Triassic–Jurassic climate in continental high-latitude Asia was dominated by obliquity-paced variations (Junggar Basin, Ürümqi, China). *Proc. Nat. Acad. Sci.*, **112**, 3624–3629.

Skarke, A., Ruppel, C., Kodis, M., Brothers, D. and **Lobecker, E. (2014)** Widespread methane leakage from the sea floor on the northern US Atlantic margin. *Nature*, **7**, 657–661.

Smith, D.G. (1989) Stratigraphic correlation of presumed Milankovitch cycles in the Blue Lias (Hettangian to earliest Sinemurian), England. *Terra Nova*, **1**, 457–460.

Suan, G., Pittet, B., Bour, I., Mattioli, E., Duarte, L.V. and **Mailliot, S.** (2008) Duration of the Early Toarcian carbon isotope excursion deduced from spectral analysis: Consequence for its possible causes. *Earth and Planet. Sci. Lett.*, **267**, 666–679.

Suan, G., van de Schootbrugge, B., Adatte, T., Fiebig, J. and **Oschmann, W.** (2015) Calibrating and magnitude of the Toarcian carbon cycle perturbation. *Paleoceanography*, **30**, PA2758, doi: 10.1002/2014PA002758.

Svensen H., Planke S., Chevallier L., Malthe-Sorenssen A., Corfu F. and **Jamtveit B.** (2007) Hydrothermal venting of greenhouse gases triggering Early Jurassic global warming. *Earth and Planet. Sci. Lett.*, **256**, 554–566.

Talukder, A.R. (2012) Review of submarine cold seep plumbing systems: leakage to seepage and venting. *Terra Nova*, **24**, 255–272.

Tryon, M.D., Brown, K.M. and **Torres, M.E.** (2002) Fluid and chemical fluxes in and out of sediments hosting methane hydrate deposits on hydrate Ridge, OR, II: Hydrological processes. *Earth and Planet. Sci. Lett.*, **201**, 541–557.

Tyson, R.V. (1995) Sedimentary Organic Matter: Organic Facies and Palynofacies. Chapman & Hall, London.

Ullmann, C.V., Thibault, N.R., Ruhl, M., Hesselbo, S.P. and **Korte, C.** (2014) Effect of a Jurassic oceanic anoxic event on belemnite ecology and evolution. *Proc. Nat. Acad. Sci.*, **111**, 10073–10076

van de Schootbrugge, B., Harazim, D., Sorichter, K., Oschmann, W., Fiebig, J., Püttmann, W., Peinl, M., Zanella, F., Teichert, B.M.A., Hoffmann, J., Stadnitskaia, A. and **Rosenthal, Y.** (2010) The enigmatic ichnofossil *Tisoa siphonalis* and widespread authigenic seep carbonate formation during the Late Pliensbachian in southern France. *Biogeosciences*, **7**, 3123–3138.

van de Schootbrugge, B., Tremolada, F., Rosenthal, Y., Bailey, T.R., Feist-Burkhardt, S., Brinkhuis, H., Pross, J., Kent, D.V. and **Falkowski, P.G.** (2007) End-Triassic calcification crisis and blooms of organic-walled disaster species. *Palaeogeogr. Palaeoclimatol. Palaeoecol.*, **244**, 126–141.

Vigran, J.O., Mørk, A., Forsberg, A.W., Weiss, H.M. and **Weitschat, W.** (2008) *Tasmanites* algae—contributors to the Middle Triassic hydrocarbon source rocks of Svalbard and the Barents Shelf. *Polar Research*, **27**, 360–371.

Walter Anthony, K.M., Anthony, P., Grosse, G. and **Chanton, J.** (2012) Geologic methane seeps along boundaries of Arctic permafrost thaw and melting glaciers. *Nat. Geosci.*, **5**, 419–426.

Warrington, G., Cope, J.C.W. and **Ivimey-Cook, H.C.** (2008) The St Audrie's Bay — Doniford Bay section, Somerset, England: updated proposal for a candidate Global Stratotype Section and Point for the base of the Hettangian Stage, and of the Jurassic System. *International Subcommission on Jurassic Stratigraphy Newsletter*, **35**, 2–66.

Waterhouse, H.K. (1999) Orbital forcing of palynofacies in the Jurassic of France and the United Kingdom. *Geology*, **27**, 511–514.

Weedon, G.P. (1986) Hemi-pelagic shelf sedimentation and climatic cycles: the basal Jurassic (Blue Lias) of South Britain. *Earth and Planet. Sci. Lett.*, **76**, 321–335.

Weedon, G.P., Jenkyns, H.C., Coe, A.L. and **Hesselbo, S.P.** (1999) Astronomical calibration of the Jurassic time-scale from cyclostratigraphy in British mudrock formations. *Philos. Trans. R. Soc. Lond.*, **357**, 1787–1813.

Whiteside, J.H., Olsen, P.E., Eglinton, T., Brookfield, M.E. and **Sambrotto, R.N.** (2010) Compound-specific carbon isotopes from Earth's largest flood basalt eruptions directly linked to the end-Triassic mass extinction. *Proc. Nat. Acad. Sci. USA*, **107**, 6721–6725.

Whittaker, A. and **Green, G.W.** (1983) Geology of the country around Weston-super-Mare. Memoir of the Geological Survey of Great Britain, *sheet 279 with parts of 263 and 295*.

Wignall, P.B. (1994) Black Shales. Issue 30 of Oxford monographs on geology and geophysics, Volume 30 of Oxford Science Publications. Clarendon Press, the University of Michigan. ISBN 0-19-854038-8, pp127.

Wood, G.D., Gabriel, A.M. and **Lawson, J.C.** (1996) Palynological techniques – processing and microscopy. In *Palynology: Principles and Applications* v 1 (Eds J. Jansonius & D.C. McGregor) pp. 29–50. American Association of Stratigraphic Palynologists Foundation, Dallas, Texas.

Wotzlaw, J.-F., Guex, J., Bartolini, A., Gallet, Y., Krystyn, L., McRoberts, C.A., Taylor, D., Schoene, B. and **Schaltegger, U.** (2014) Towards accurate numerical calibration of the Late Triassic: High precision U-Pb geochronology constraints on the duration of the Rhaetian. *Geology*, **42**, 571.

Zachos, J.C., McCarren, H., Murphy, B., Röhl, U. and **Westerhold, T.** (2010) Tempo and scale of late Paleocene and early Eocene carbon isotope cycles: Implications for the origin of hyperthermals. *Earth and Planet. Sci. Lett.*, **299**, 242–249.

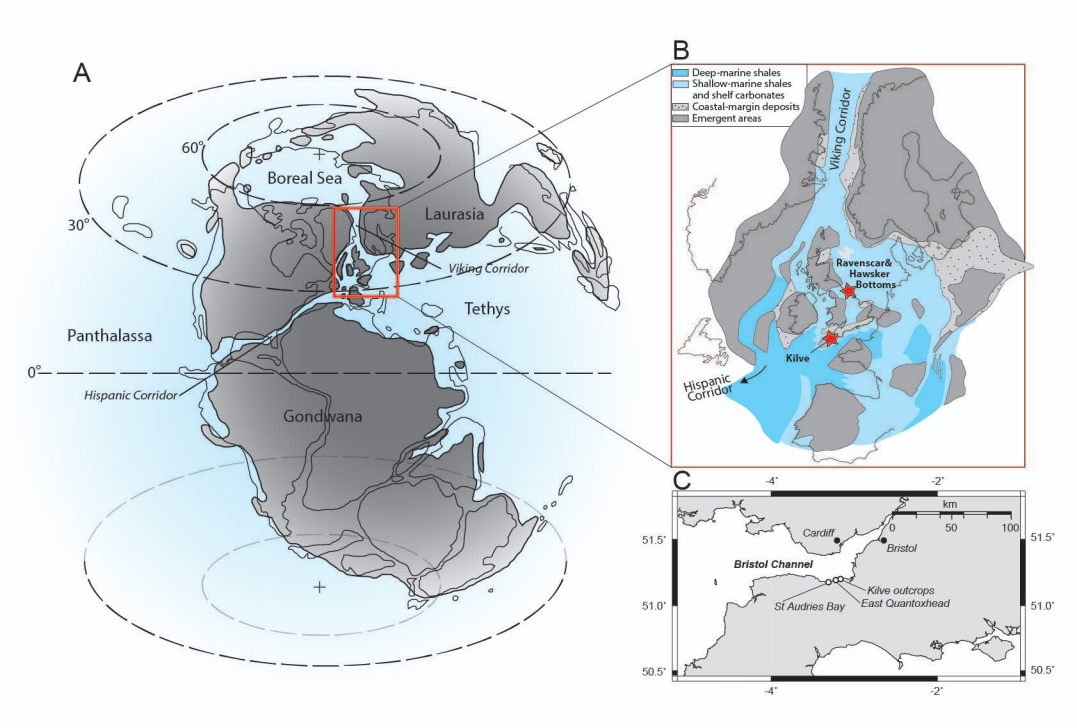
A
60°
30°
0°
Boreal Sea
Laurasia
Viking Corridor
Tethys
Panthalassa
Hispanic Corridor
Gondwana
B
Deep-marine shales
Shallow-marine shales and shelf carbonates
Coastal-margin deposits
Emergent areas
Viking Corridor
Ravenscar& Hawsker Bottoms
Kilve
Hispanic Corridor
C
-4°
-2°
km
0
50
100
51.5°
51.0°
50.5°
Cardiff
Bristol
Bristol Channel
Kilve outcrops
St Audries Bay
East Quantoxhead

Bristol Channel Basin:
St Audries Bay and East Quantoxhead (UK)

(Hesselbo et al., 2002; Ruhl et al., 2010; Hüsing et al., 2014)

Bristol Channel Basin: East Quantoxhead (UK)

(Ruhl et al., 2010; Hüsing et al., 2014)

Bristol Channel Basin: Kilve (UK)

(This study)

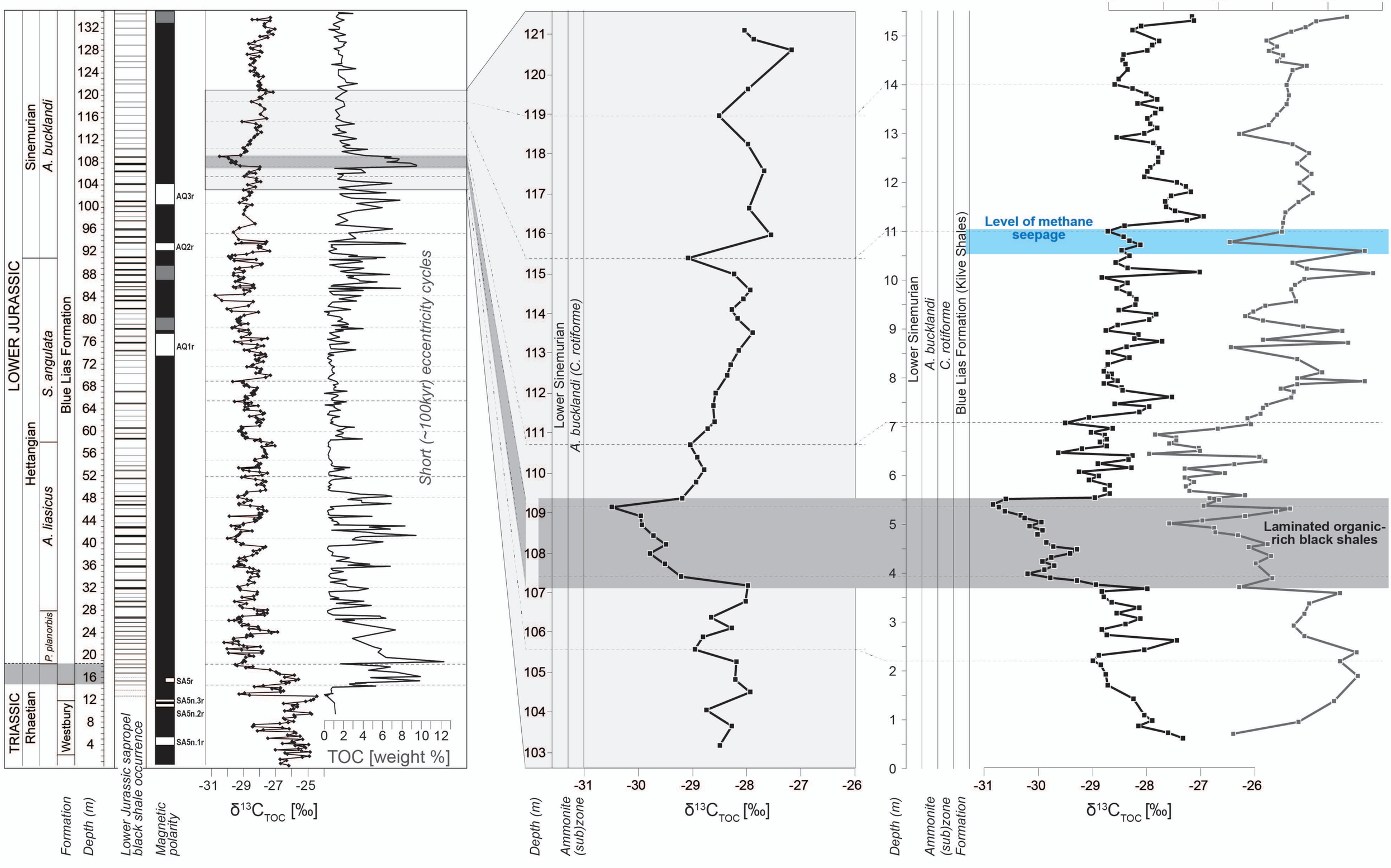

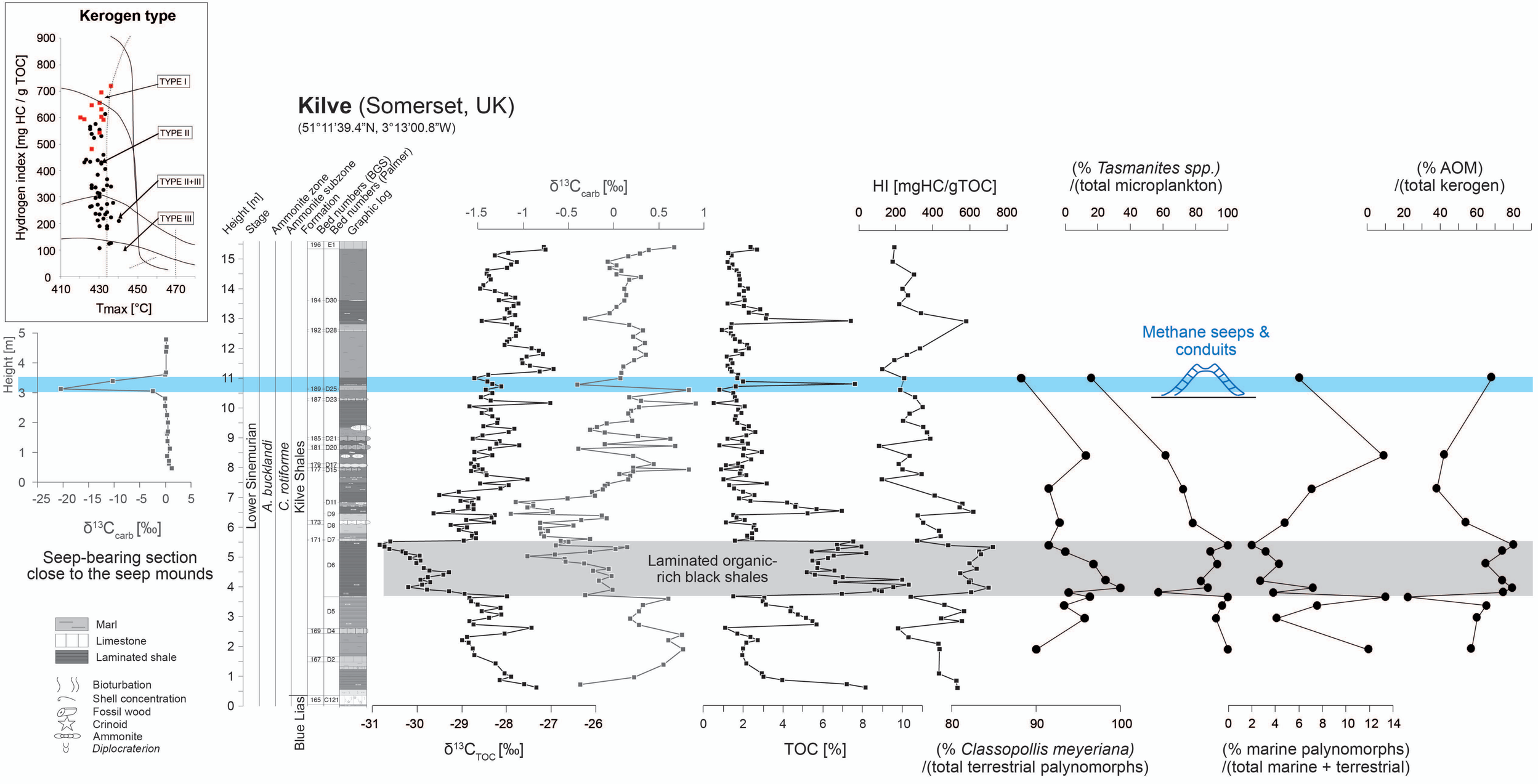
Kerogen type
Hydrogen index [mg HC / g TOC]
Tmax [°C]
TYPE I
TYPE II
TYPE II+III
TYPE III
Kilve (Somerset, UK)
(51°11'39.4"N, 3°13'00.8"W)
Height [m]
Stage
Ammonite zone
Ammonite subzone
Formation
Bed numbers (BGS)
Bed numbers (Palmer)
Graphic log
Lower Sinemurian
A. bucklandi
C. rotiforme
Kilve Shales
Blue Lias
δ13Ccarb [‰]
HI [mgHC/gTOC]
(% Tasmanites spp.) /(total microplankton)
(% AOM) /(total kerogen)
Methane seeps & conduits
Laminated organic-rich black shales
Seep-bearing section close to the seep mounds
Marl
Limestone
Laminated shale
Bioturbation
Shell concentration
Fossil wood
Crinoid
Ammonite
Diplocraterion
δ13CTOC [‰]
TOC [%]
(% Classopollis meyeriana) /(total terrestrial palynomorphs)
(% marine palynomorphs) /(total marine + terrestrial)

Kilve (Somerset, UK)

(51°11'39.4"N, 3°13'00.8"W)

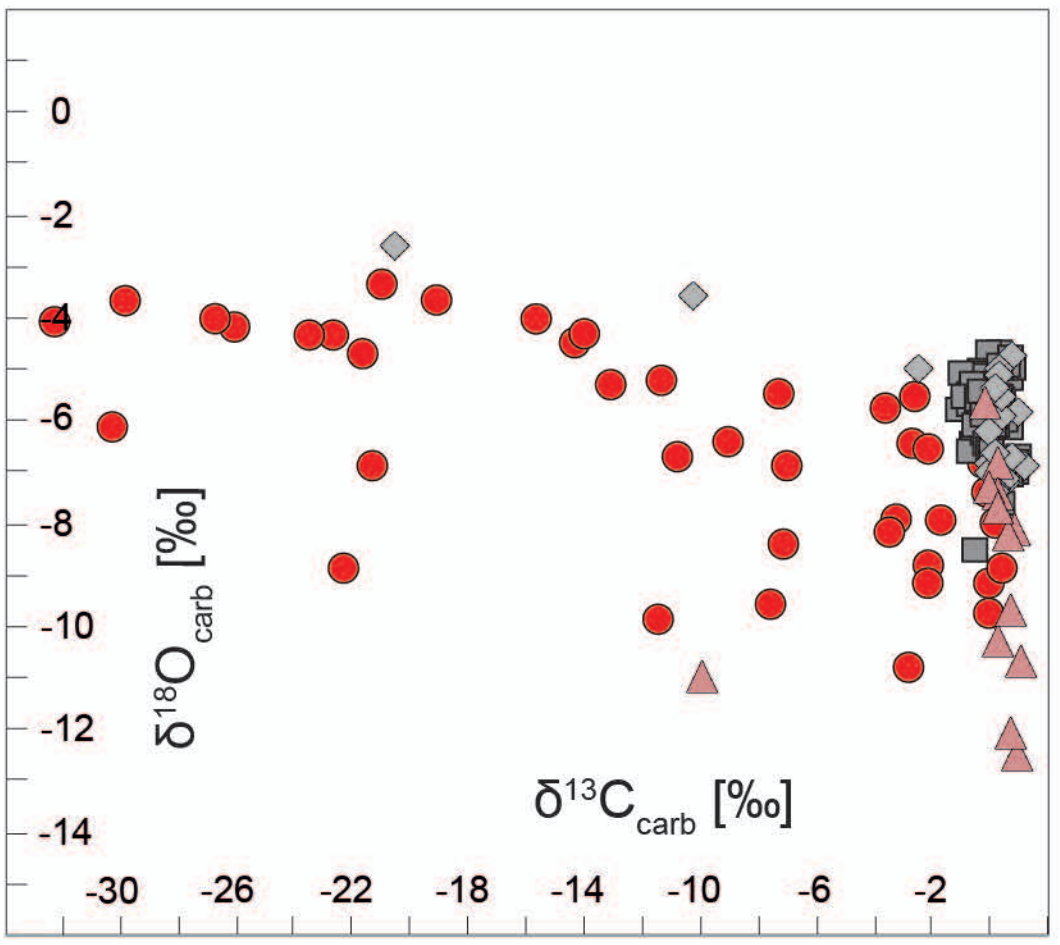

Ravenscar (Yorkshire, UK)

(54°24'29.3"N, 0°29'32.7"W)

- $\delta^{13}C_{carb}$ and $\delta^{18}O_{carb}$ of the Lower Sinemurian (Kilve) and Lower Toarcian (Ravenscar) methane-seep mounds (Allison *et al.*, 2008; Price *et al.*, 2008; this study)
- $\delta^{13}C_{carb}$ and $\delta^{18}O_{carb}$ of time-equivalent Lower Sinemurian (Kilve) and Lower Toarcian (Hawsker Bottoms) bulk-rock and belemnites (This study; McArthur *et al.*, 2000))
- $\delta^{13}C_{carb}$ and $\delta^{18}O_{carb}$ of the Lower Sinemurian (Kilve) mound-bearing section very close to the seep mounds (Allison *et al.*, 2008)
- $\delta^{13}C_{carb}$ and $\delta^{18}O_{carb}$ of the bulk rock from the same stratigraphic level of the methane seeps, but different distance (Price *et al.*, 2008)

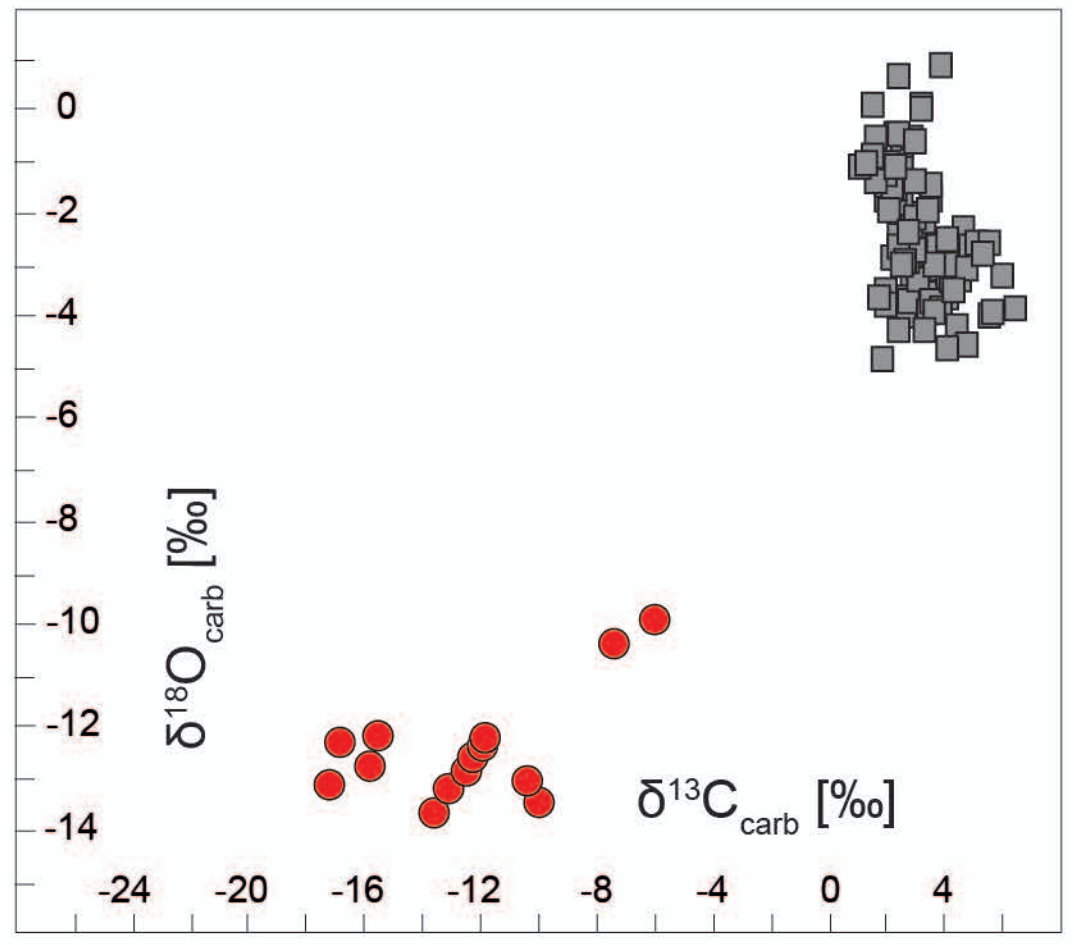

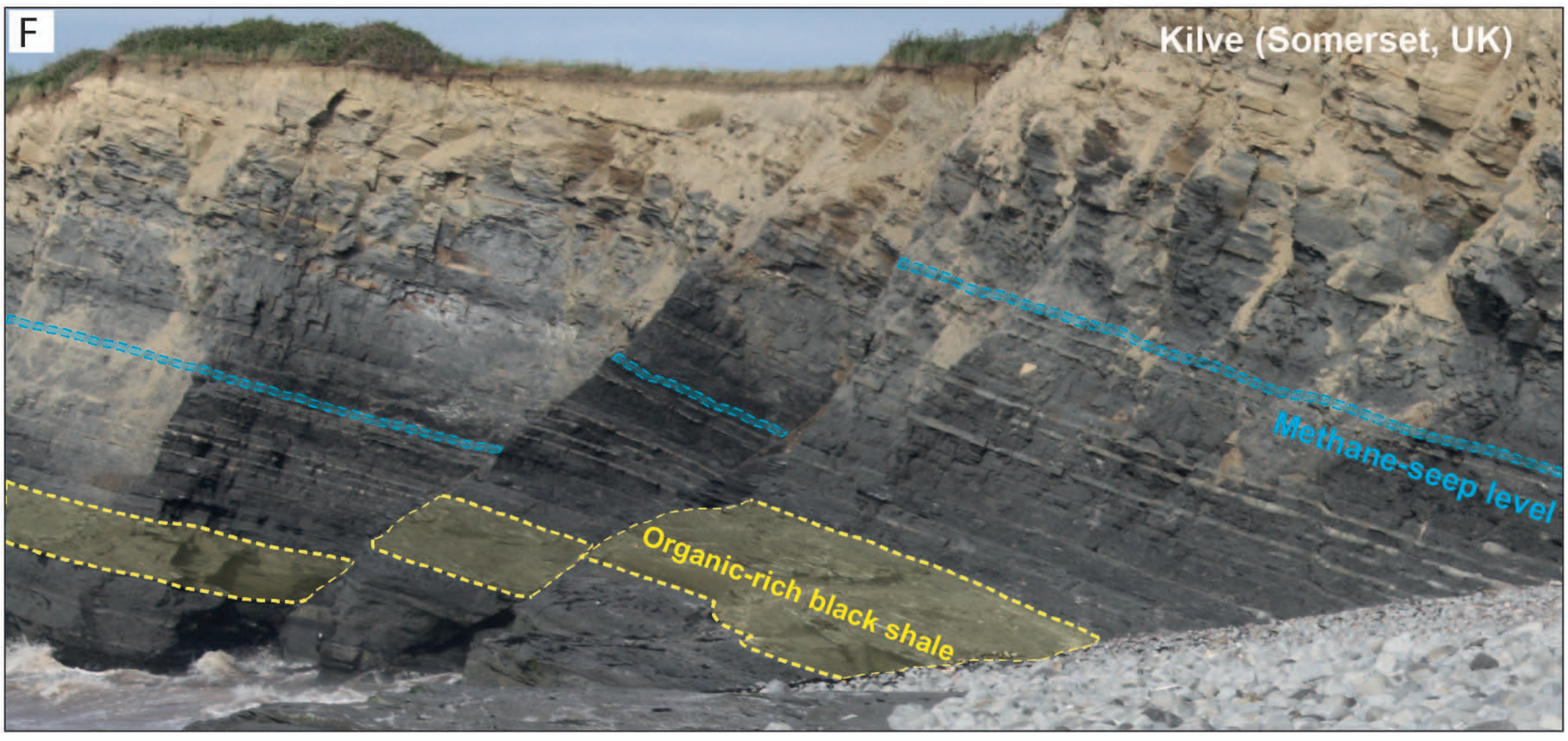

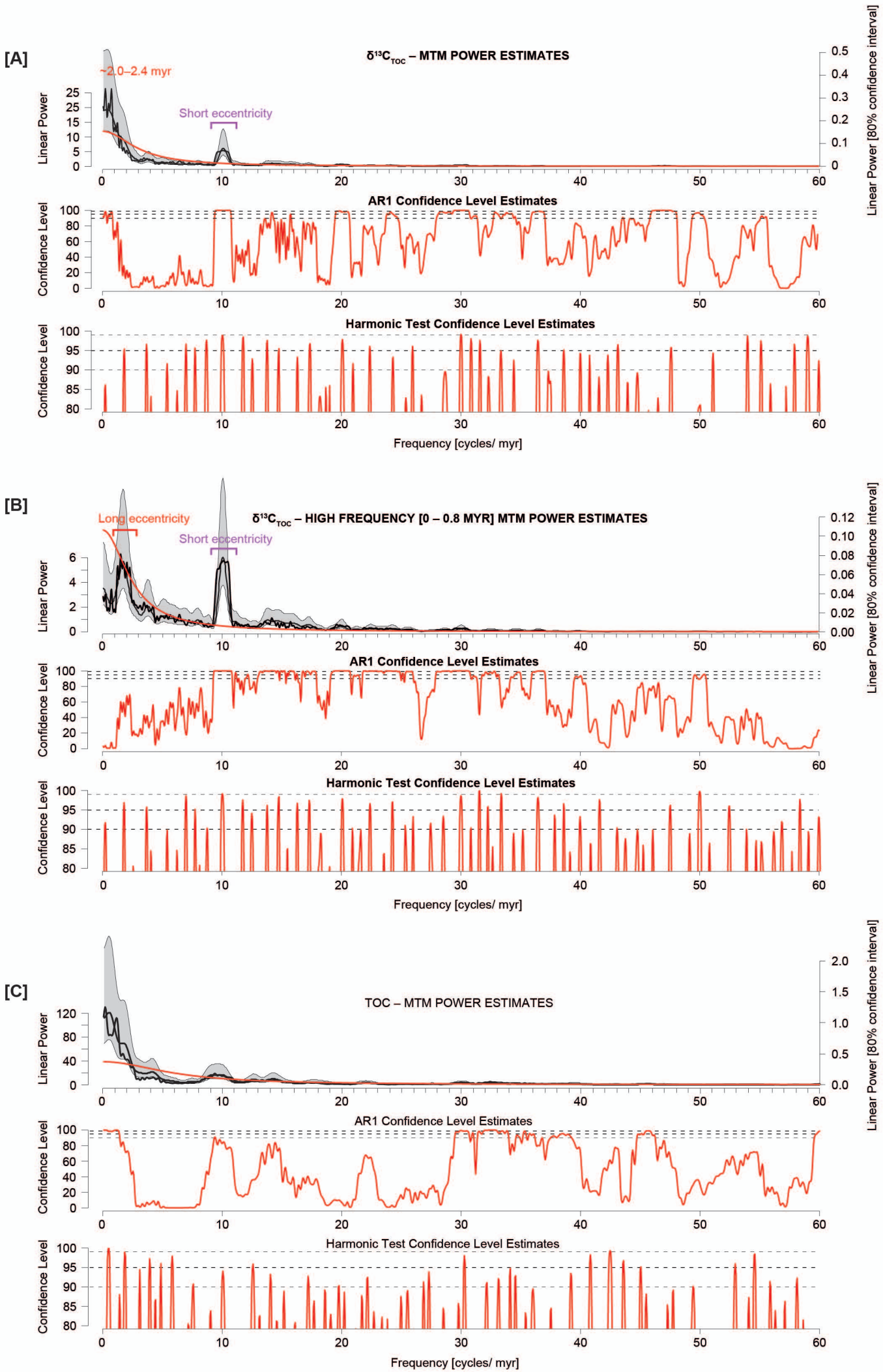
[A]
δ13CTOC – MTM POWER ESTIMATES
~2.0–2.4 myr
Short eccentricity
Linear Power
Linear Power [80% confidence interval]
AR1 Confidence Level Estimates
Confidence Level
Harmonic Test Confidence Level Estimates
Frequency [cycles/ myr]
[B]
δ13CTOC – HIGH FREQUENCY [0 – 0.8 MYR] MTM POWER ESTIMATES
Long eccentricity
Short eccentricity
Linear Power
Linear Power [80% confidence interval]
AR1 Confidence Level Estimates
Confidence Level
Harmonic Test Confidence Level Estimates
Frequency [cycles/ myr]
[C]
TOC – MTM POWER ESTIMATES
Linear Power
Linear Power [80% confidence interval]
AR1 Confidence Level Estimates
Confidence Level
Harmonic Test Confidence Level Estimates
Frequency [cycles/ myr]

La2010

The Laskar et al., (2011) astronomical solutions and the filtered ~405 kyr component.

La2010a
La2010b
La2010c
La2010d

~405 kyr cycles numbered back from present:

489 490 491 492 493 494 495 496 497

2–2.8 myr component:

~405 kyr eccentricity component:

Eccentricity solutions:

198.2 198.4 198.6 198.8 199.0 199.2 199.4 199.6 199.8 200.0 200.2 200.4 200.6 200.8 201.0 201.2 201.4 201.6 201.8 202.0

Absolute time [Ma]

Radiometric ages for the end-Triassic mass extinction and the Triassic–Jurassic and Hettangian–Sinemurian boundaries from: the Newark and Hartford Basin (USA, the Fundy Basin (Canada), the Pucara Basin (Peru) and from New York Canoyn (USA)

End-Triassic mass extinction

Bristol Channel Basin (UK)

~405 kyr and the modulated short (~100kyr) eccentricity filter

Thin black line: Data
Thick grey line: 5-point moving average

TOC [%]: 0 2 4 6 8 10 12

Lower Jurassic sapropel black shale occurrence

~405 kyr and the modulated short (~100kyr) eccentricity filter

Thin black line: Data
Thick grey line: 5-point moving average

$\delta^{13}C_{TOC}$ [‰]: -24 -25 -26 -27 -28 -29 -30 -31

AQ3r AQ2r AQ1r SA5r SA5n.3r SA5n.2r SA5n.1r

Magnetic polarity

Numerical time [Ma]

198.3 198.5 198.7 198.9 199.1 199.3 199.5 199.7 199.9 200.1 200.3 200.5 200.7 200.9 201.1 201.3 201.5 201.7

Blue Lias Formation | Westb. Fm.

Ammonite zonation

A. bucklandi	S. angulata	A. liasicus	P. planorbis
Sinemurian	Hettangian		Rhaetian
LOWER JURASSIC			UPPER TRIASSIC

Newark and Hartford Basin (USA) and Fundy Basin (Canada)

~405 kyr eccentricity modulated short (~100kyr) eccentricity cycle

Relative time [kyr]: 2500 2000 1500 1000 500 0 -100

Lake-bed occurence

Magnetic polarity: H26r H25r H24r

Depth [m]: 2500 2000 1500 1000 500 0

Sinemurian | Hettangian | Rhaetian
LOWER JURASSIC | UPPER TRIASSIC

Radiometric Age

[H] 201.52±0.034 Ma *(reference in figure caption)*

Pucara Basin (Peru)

Radiometric Ages *(references in figure caption)*

[A] 199.43±0.10 Ma/ **199.53±0.19 Ma**
[B] 200.35±0.13 Ma
[C] 200.67±0.21 Ma
[D] 201.26±0.13 Ma/ **201.29±0.16 Ma**
[E] 201.35±0.10 Ma/ **201.36±0.13 Ma**
[F] 201.45±0.16 Ma/ **201.40±0.18 Ma**/ 201.58±0.17 Ma
[G] 201.78±0.16 Ma

Radiometric ages

Ammonite occurrence: A *B. canadensis*; *Angulaticeras*; B *Kammerkarites*; *Alsatites*; C *P. tilmanni*; D; E; F FO *P. spelae*; G LO *C. crickmayi*

Depth [m]: 140 130 120 110 100 90 80 70 60 50

Ammonite zonation

S. angulata	A. liasicus	P. planorbis	C. marshi
Sinemurian	Hettangian		Rhaetian
LOWER JURASSIC			UPPER TRIASSIC

New York Canyon (USA)

Radiometric Age *(reference in figure caption)*

[I] 201.33±0.13

I FO *P. spelae* LO *C. crickmayi*

Hettangian | Rhaetian
LOWER JURASSIC | U. TRIASS.

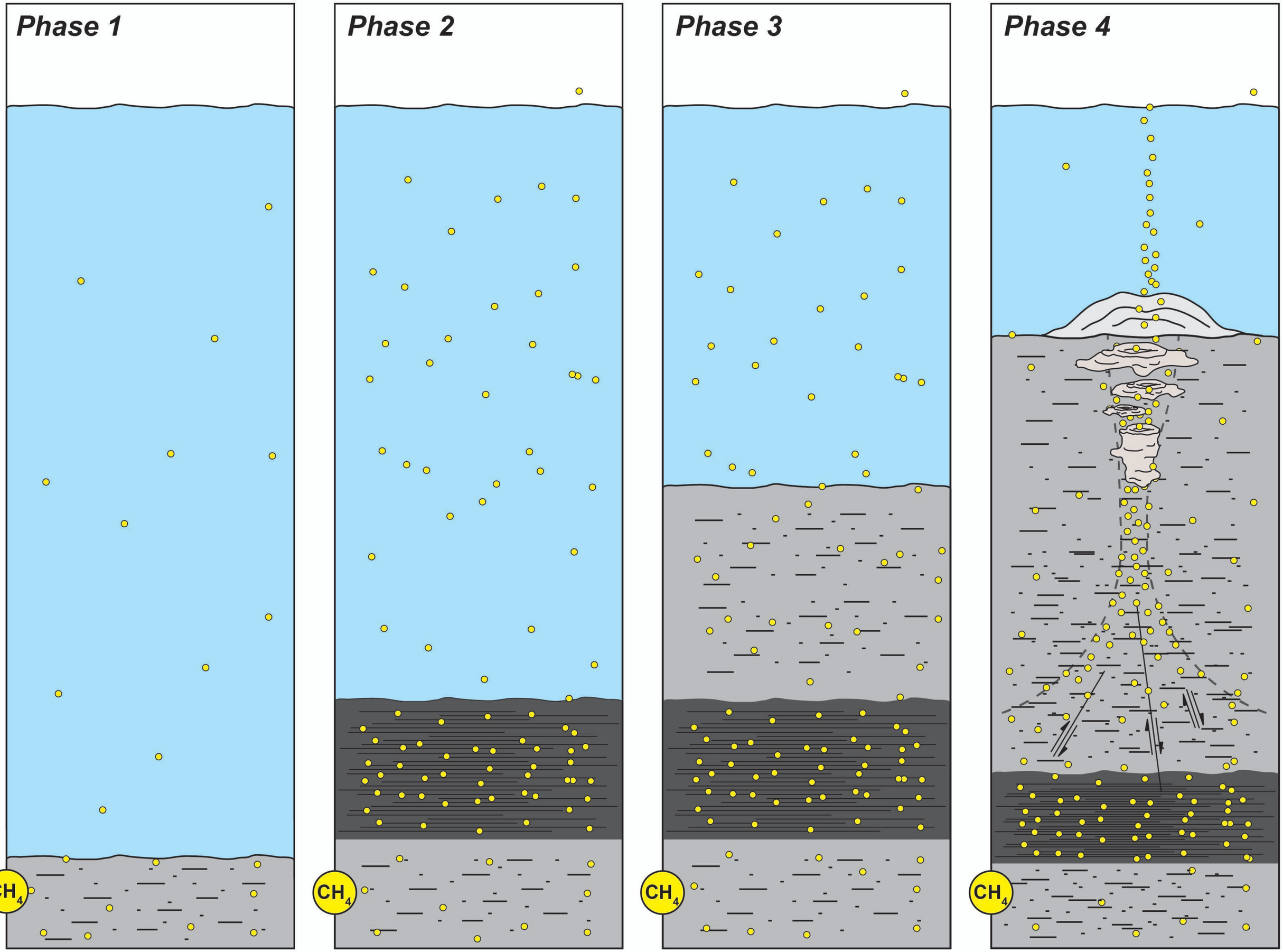
Phase 1
Phase 2
Phase 3
Phase 4
CH4
CH4
CH4
CH4
Organic-lean mudstone
Organic-rich laminated black shale
CH4
Sedimentary biogenic methane formation
Methane seep
Faulting (compaction/lithification)

SOMERSET (UK): ***Sinemurian***

Kilve

(51°11’39.4”N, 3°13’00.8”W)

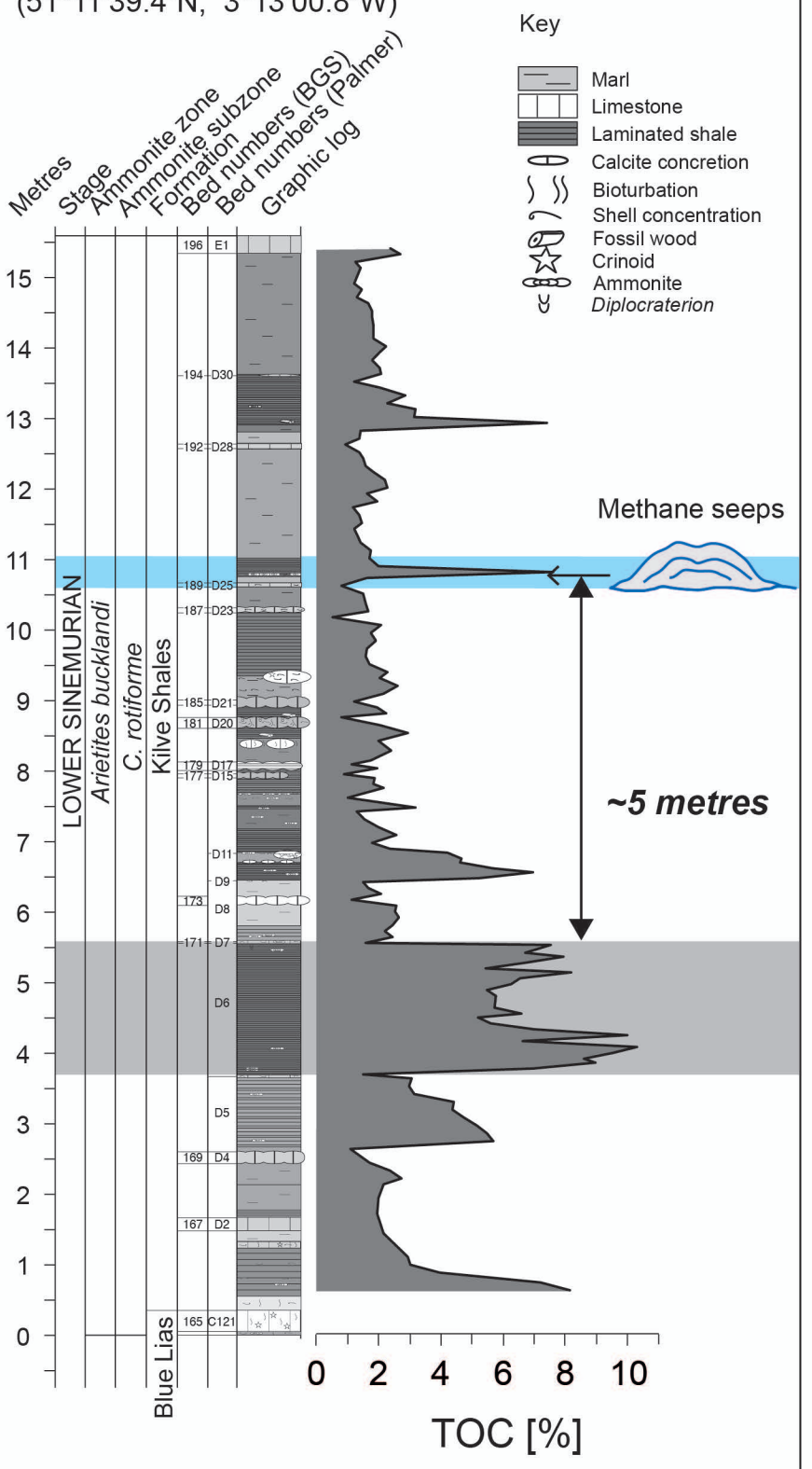

YORKSHIRE (UK): ***Toarcian***

Hawsker Bottoms

(Kemp *et al.*, 2011)

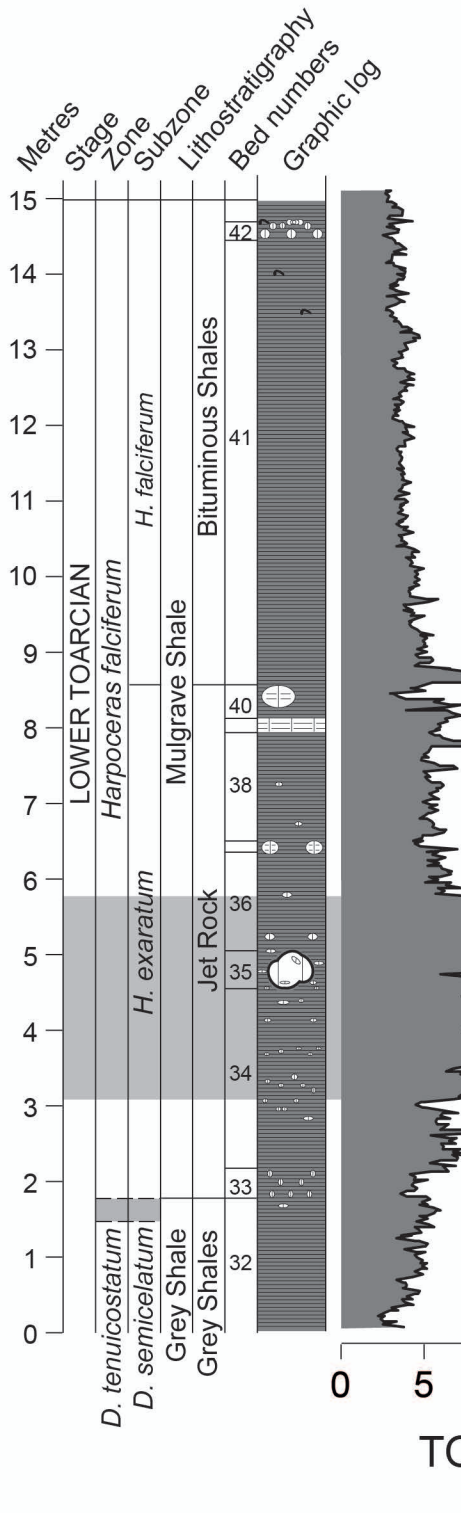

Ravenscar

(54°24’29.3”N, 0°29’32.7”W)